



## **School of Chemistry**

Diamond Chemical Vapour Deposition Using Static Flow Methods

Mujtaba Abbas

**This thesis is submitted in partial fulfilment of the requirements for the Honours  
Degree of MSci at the University of Bristol**

Neil Fox

Paul May

Physical and Theoretical Group

## **Contents**

<b>1</b>	<b>Abstract</b> .....	iv
<b>2</b>	<b>Acknowledgements</b> .....	v
<b>3</b>	<b>Introduction</b> .....	1
<b>3.1</b>	<b>Properties and Structure of Diamond</b> .....	1
<b>3.2</b>	<b>Chemistry of Chemical Vapour Deposition (CVD)</b> .....	3
<b>3.3</b>	<b>CVD Methods</b> .....	6
<b>3.4</b>	<b>Project Context</b> .....	10
<b>3.5</b>	<b>PDR</b> .....	11
<b>3.6</b>	<b>Single Crystal Growth</b> .....	12
<b>3.7</b>	<b>Static Flow</b> .....	14
<b>3.8</b>	<b>Characterisation</b> .....	14
<b>3.8.1</b>	<b>Optical Emission Spectroscopy (OES)</b> .....	15
<b>3.8.2</b>	<b>Raman Spectroscopy</b> .....	15
<b>3.8.3</b>	<b>Scanning Electron Microscopy (SEM)</b> .....	17
<b>3.9</b>	<b>Taguchi Method</b> .....	18
<b>4</b>	<b>Experimental Method</b> .....	20
<b>4.1</b>	<b>Experiments and Aims</b> .....	20
<b>4.2</b>	<b>Seeding</b> .....	20
<b>4.3</b>	<b>Reactor Design</b> .....	21
<b>4.4</b>	<b>Reactor Operation</b> .....	22
<b>4.4.1</b>	<b>Continuous Flow Start</b> .....	22
<b>4.4.2</b>	<b>Static Flow Start</b> .....	23
<b>4.4.3</b>	<b>Shutting Down</b> .....	23
<b>4.5</b>	<b>Residual Doping</b> .....	23
<b>4.6</b>	<b>Test</b> .....	24
<b>5</b>	<b>Characterisation</b> .....	24
<b>5.1</b>	<b>OES</b> .....	24
<b>5.2</b>	<b>Raman Spectroscopy</b> .....	25
<b>5.3</b>	<b>Scanning Electron Microscopy</b> .....	26
<b>6</b>	<b>Results and Discussion</b> .....	27
<b>6.1</b>	<b>OES</b> .....	27
<b>6.1.1</b>	<b>Test</b> .....	29

6.1.2	4% and 6% Residually-Doped Data.....	29
6.1.3	4 % Undoped Data.....	32
6.1.4	Undoped 6 % .....	33
6.1.5	Time Constants.....	34
6.1.6	Overall.....	34
6.2	Raman Spectroscopy .....	35
6.2.1	Undoped 6 % Data Set.....	36
6.2.2	Undoped 4 % Data Set.....	37
6.2.3	Residually-doped 4 % .....	38
6.2.4	Residually-doped 6 % .....	39
6.2.5	Overall.....	40
6.3	Scanning Electron Microscopy .....	40
6.3.1	6 % Residually-Doped .....	41
6.3.2	6 % Undoped .....	42
6.3.3	4 % Undoped .....	43
6.3.4	4 % Residually-Doped .....	44
6.3.5	Overall.....	44
7	Conclusions.....	45
8	References.....	47
9	Appendix.....	50
9.1	Section A - PDR.....	50
9.2	Section B -OES .....	53
9.3	Raman Analysis Data and Spectra .....	56
9.4	Section D- SEM Images .....	59

## **Growth of Isotope Pure Diamond Film by Static Flow**

### **1 Abstract**

This research focuses on diamond growth, using a zero-gas flow environment with a methane and hydrogen gas mixture. Variations on the static flow process were investigated where the gas mixture was periodically introduced in 30 second pulses every 30, 40, 60 and 120 minutes, with each run being 2 hours long. For each process cycle methane concentration was varied using 4 % and 6 % methane in hydrogen. Chamber conditions were also varied between an undoped chamber and a residually-boron doped chamber to study the impact of dopant impurities upon growth conditions. The resultant diamond films were characterised using scanning electron microscopy and Raman spectroscopy. Optical emission spectroscopy was used as a process monitor for each growth run. Results had shown that growth rate, purity and crystallinity varied depending on which method and conditions were used. Based upon a small set of experimental data it was found that

Static flow chemical vapour deposition is applicable to the eventual fabrication of a diamond battery. This requires synthesis of carbon-14 diamond layers. Carbon-14 methane is highly radioactive and very expensive, therefore, the ability to grow high quality films with as small amounts of C-14 methane as possible would be safer and more cost effective. This research has shown good quality diamond can be grown using static flow depending on the specific conditions and methods chosen.

## 2 Acknowledgements

I would like to thank everyone in the diamond group for their help during this project. In particular help from Dr James Smith and Ed Smith has been very much appreciated. Guidance from Professor Paul May and Professor Neil Fox was very helpful during the course of this project.

I would like to thank my family for their support. Especially with their diamond synthesis history having made one 22 years ago.

505, LB8 and especially KM11 helped me grow my favourite diamonds.

### 3 Introduction

#### 3.1 Properties and Structure of Diamond

Much research has gone into the growth of synthetic diamond using chemical vapour deposition (CVD) since the 1980s. This is because of the numerous potential functions of large diamond layers.<sup>1</sup> The exceptional properties of diamond are the main reason for this effort. Diamond can be manufactured into cutting and grinding tools due to its characteristic hardness and robustness.<sup>2</sup> These tools have a myriad of industrial uses, some examples being within the automotive industry to shape car and engine parts. Furthermore, another use for the strength of diamond is when it is used to engrave hard materials such as granite with little or no damage.<sup>3</sup>

Properties of diamond such as its high thermal conductivity have also fuelled research into diamond growth. Materials with high thermal conductivity have a multitude of industrial applications. For example, acting as heat sinks for power plants, solar thermal water systems and general heat regulation in electronic devices. Natural diamond single crystals are reported to have conductivity of  $24\text{-}25 \text{ W cm}^{-1} \text{ K}^{-1}$ . Isotopically pure carbon-12 synthetic single crystals have a higher value of  $33 \text{ W cm}^{-1} \text{ K}^{-1}$ .<sup>4</sup> Diamond has the highest known thermal conductivity over 100 Kelvin with synthetic diamond boasting better values.<sup>4</sup> Diamonds role in electronics is extended by its wide band-gap of 5.47 eV where it can be doped and can play an active role in electronic applications.<sup>5,6</sup>

**Table 1** Properties and applications of diamond.<sup>7</sup>

<b>Property</b>	<b>Value</b>	<b>Applications</b>
<b>Hardness</b>	90 GPa	Cutting Tools
<b>Coefficient of Friction</b>	0.05	Low Friction Coatings
<b>Thermal Conductivity</b>	20 W/mK	Heat Sinks
<b>Chemical Reactivity</b>	Inert	Electrochemistry
<b>Thermal Expansion</b>	$0.8 \times 10^{-6} \text{ K}^{-1}$	
<b>Bulk Modulus</b>	$1.2 \times 10^{12} \text{ Nm}^{-3}$	High Strength Materials
<b>Dielectric Constant</b>	5.5	Electronics
<b>Band Gap</b>	5.45 eV	Electronics
<b>Optical</b>	Transparent from deep UV to far IR	Optical Windows and Coatings
<b>Electrical Resistivity</b>	$10^{13} \Omega$	Electronics

Diamonds exceptional electronic properties lead some researchers to describe it as the ‘crown jewel’ for electronic devices.<sup>8</sup> Single crystal diamond can have a reported mobility of  $4500 \text{ cm}^2 \text{ V}^{-1} \text{ S}^{-1}$  and  $3800 \text{ cm}^2 \text{ V}^{-1} \text{ S}^{-1}$  electron and hole mobilities respectively.<sup>6</sup> These are the highest mobilities of any wide band gap semiconductor. Having a wide band-gap is beneficial for electronic devices because they can handle higher voltages, powers and operating temperatures. Having a wide band gap also means having a high electric breakdown potential. This is very useful in the manufacture of electronic devices such as Schottky diodes. Schottky diodes have a switching function and current can be turned on or off

depending on the direction that voltage is applied. Schottky diodes cause current to flow in one direction and is characterised by its low forward voltage and fast switching ability.<sup>9</sup> The higher the breakdown voltage, the smaller it is possible to manufacture Schottky devices with faster switching. Therefore, with diamond having an extraordinarily high breakdown voltage, it would make high performance Schottky diodes. This could improve the future of high power devices and improve the efficiency of solar cells.<sup>9</sup> Other applications of diamonds electronic properties are room temperature quantum computing, bio-sensing, high radiation and particle detectors.<sup>10</sup>

The optical properties of diamond like as its high refractive index of 2.4 and broad optical transparency, give it a wide range of applications such as for optical windows.<sup>5,11</sup> Optical windows play an important role in fusion reactors. CVD diamond being the only material that can handle the power generated when a plasma is heated to temperatures required for fusion. In addition to this, diamond can be used for attenuated total reflectance spectroscopy (ATR) due to its high refractive index.<sup>12</sup> ATR is a frequently used sampling technique for FTIR spectroscopy.

Using chemical vapour deposition techniques, diamond can be grown with high quality and size control. As a result, CVD diamond has many more industrial uses such as the manufacture of diamond electrodes and radiation detectors.<sup>2</sup> One further potential use of high quality, large area CVD diamond is in radio-voltaic batteries that harvest beta or gamma radiation to generate micro-power for remote sensing and health monitoring of geological and man-made structures.<sup>13</sup>

The extraordinary properties of diamond are attributed to its structure. Diamond consists of a cubic close packed crystal structure. Each carbon is  $sp^3$  hybridised and forms a strong covalent bond with four of its nearest neighbours, giving a tetrahedral structure. Stacking these tetrahedral structures together forms the giant covalent structure of diamond.<sup>14</sup> The carbon-carbon bond length is reported as 1.544 Å and a 109.5° bond angle, characteristic of a tetrahedral structure.<sup>15</sup> Diamond's exceptional hardness is attributed to this 3-dimensional giant covalent structure with close packed carbon atoms, with the structure having tetragonal symmetry. Diamond's optical properties are also attributed to its structure with the symmetry causing the lack of infra-red activity. However, diamond has a Raman-active mode at 1332.4  $cm^{-1}$ .<sup>16</sup>

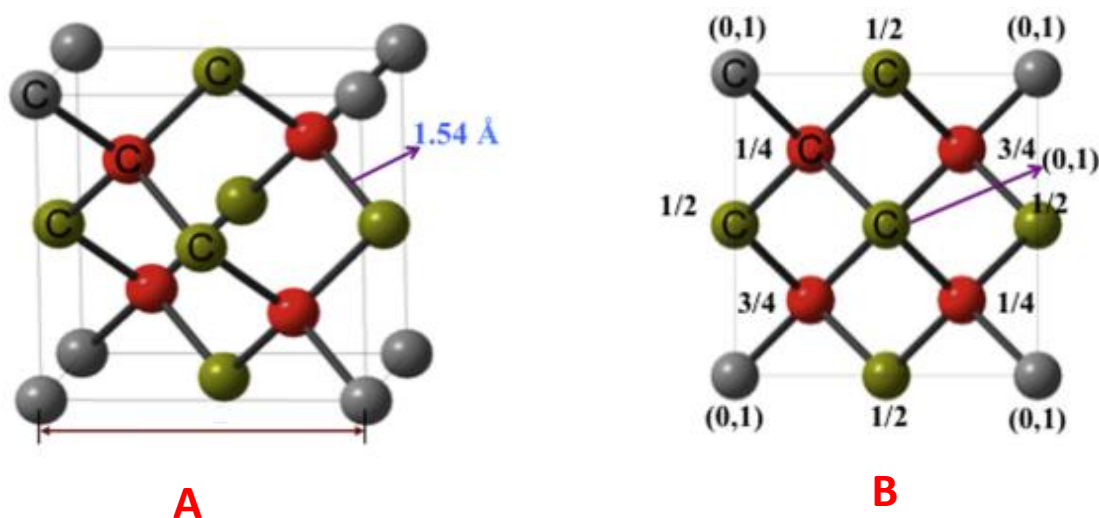


**Figure 1** A shows the unit cell structure of cubic diamond. B shows a FCC face centred cubic crystal structure. Adapted from

Chandran et al.<sup>17</sup>

### 3.2 Chemistry of Chemical Vapour Deposition (CVD)

The technique used to make diamond at low pressures is called chemical vapour deposition. This requires chemical reactions occurring in a gas phase and the species formed are deposited onto a solid surface.<sup>18</sup> There are many gas compositions that can be used for this process however, this report will focus on growth using methane, hydrogen and argon. **Figure 2** shows the chemical processes taking place using a methane and hydrogen gas mixture. In this example the gases are activated using a hot filament reactor. However, this schematic is relevant for other CVD methods, where the hot filament could be replaced by another region of activation, such as a plasma. Although,  $C_2$  radicals are shown in **figure 2** not to directly take part in depositing carbon, this being exclusively  $CH_3$  in the figure. But for high electron temperature plasmas such as the pulsed DC- plasma assisted (PDR) CVD methods,  $C_2$  may play a more prominent role in laying down carbon diamond.

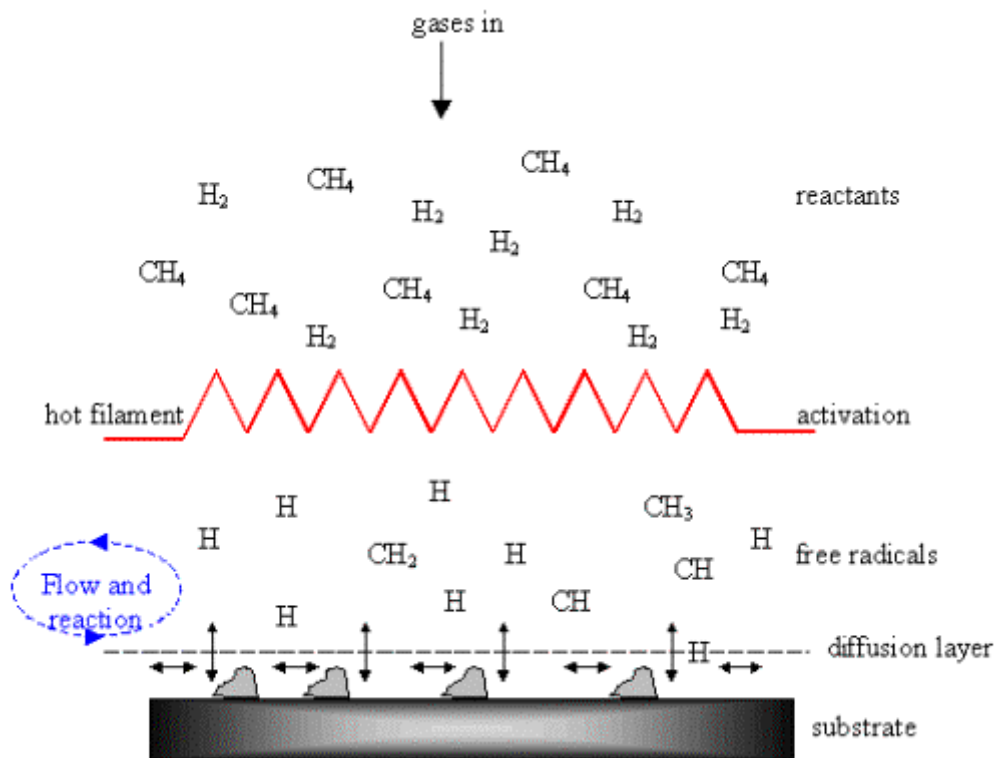


**Figure 2** Schematic diagram showing the chemistry for diamond deposition. Methane and hydrogen are activated using a hot filament. Adapted from May et al.<sup>18</sup>

## Methane

The process of chemical vapour deposition to form diamond requires the addition of  $sp^3$  carbon atoms to the substrate surface as shown in **figure 2**. Therefore, methane is the preferred feedstock used as the source of carbon atoms. Methane gas can react with atomic hydrogen to form carbon containing radicals. These radicals can then adsorb onto a substrate surface. If the carbon does not desorb and reacts with the surface, assuming the deposited carbon is  $sp^3$  hybridised, diamond growth should occur. If  $sp^2$  carbon is deposited, it can be etched using atomic hydrogen as shown in **figure 2**. When looking through the optical window of a reactor, as methane gas is added a green glow can be seen. This is characteristic of  $C_2$  swan bands. The intensity of these swan bands can be measured using optical emission spectroscopy.

## Hydrogen

The critical role of hydrogen in CVD diamond formation was discovered by Angus in the 1960s. Hydrogen increases the rate of diamond growth in several ways. Once atomic hydrogen is present following the dissociation of molecular hydrogen, it prevents critical graphite nucleation. Hydrogen concentration raises growth rate and quality by increasing the degree of surface coverage by the methyl radicals.<sup>19</sup> Additionally, if graphitic carbon was formed on the substrate surface, it could then be hydrogenated producing a  $sp^3$  carbon site from which diamond could grow. Studies show the composition of the surface at different stages of the diamond growth process. At first a graphitic carbon phase was formed, this then transferred to an hydrogenated carbon phase eventually leading to a diamond phase.<sup>20</sup> Atomic hydrogen adds to bare sites, providing a hydrogen terminated surface that inhibits surface reconstruction.<sup>2</sup> Overall, the critical role of hydrogen has many benefits, such as etching away any non-diamond carbon species created at the substrate surface.

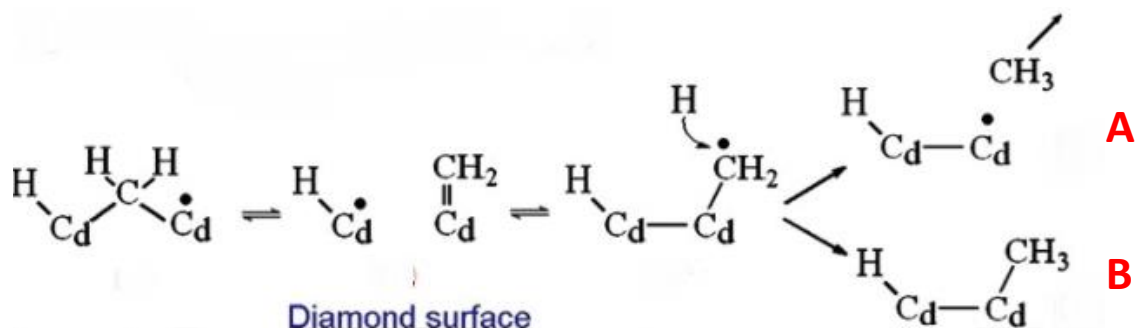


**Figure 3** The interconversion between  $sp^3$  and  $sp^2$  carbon. Following this two mechanisms can occur. Mechanism A shows etching of the  $sp^2$  carbon using atomic hydrogen. Mechanism B shows hydrogen addition which may lead to the formation of  $sp^3$  carbon without etching. Figure adapted by May et al.<sup>21</sup>

## Argon

Argon can be used as part of the gas composition for diamond growth. Using argon gas, along with methane and hydrogen, is said to improve the crystallinity and quality of the diamond deposit. Furthermore, studies have shown that the addition of argon can increase the diamond growth rate.<sup>22</sup> Alongside argon's ability to aid diamond growth, it is also used to cool down the PDR chamber vessel once the process is complete. This is because argon can cool the chamber down slowly. If air was used to cool down the reactor, it would cool too rapidly and induce oxidation on the metal surfaces. Therefore, with argon being inert and cooling the chamber slowly, it can be used once growth runs have been completed. One study stated that adding argon as part of the gas mixture promotes better grain size control of the diamond.<sup>23</sup> . Therefore, there are two argon gas lines connected to the PDR in the Bristol Diamond Lab. One has a mass flow controller that provides measured amounts of argon for gas mixtures. One without a mass flow controller that provides an arbitrary amount of gas just to cool the chamber.

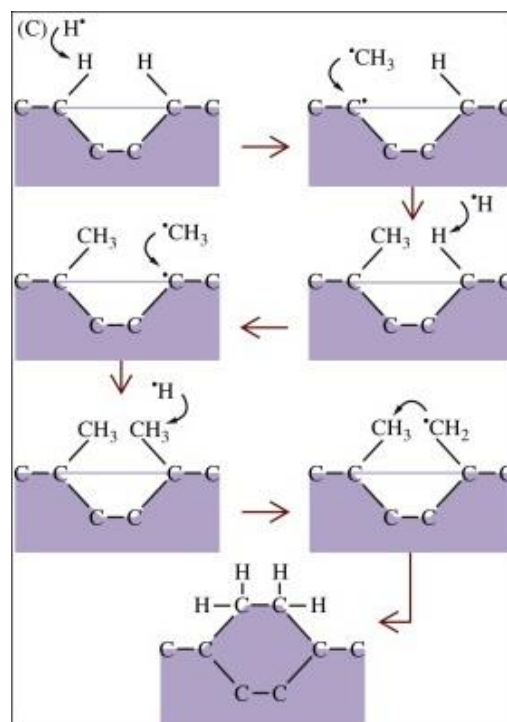


**Figure 4** Chemistry of diamond growth. Showing how attaching each carbon atom can lead to diamond growth. Adapted from Chandran et al.<sup>17</sup>

### 3.3 CVD Methods

Chemical vapour deposition is a method which requires the activation of a gas mixture, often involving methane and hydrogen. This gas mixture is activated using either thermal or plasma assisted methods. The activated region would consist of radicals and fragments of the precursor gases. Eventually, some of the radicals will chemisorb onto the substrate surface. However, chemisorption can be followed by desorption. As a result, there may be many unsuccessful adsorptions before a successful reaction occurs which can then potentially lead to the formation of diamond.<sup>18</sup>

There are several methods of activating the precursor gases. Each method has advantages and disadvantages which ultimately affect the quality and growth rate of a produced diamond film.

#### Hot Filament Reactor

Hot filament reactors thermally activate the precursor gases and requires a filament to be heated up to 2200 °C.<sup>24</sup> For this reason, either tungsten or tantalum are used as they have high melting points of 3414 °C and 3017 °C respectively.<sup>25,26</sup> The main role of the filament is to dissociate molecular hydrogen into hydrogen atoms but if methane molecules come in contact with it, they will dissociate into fragments. The atomic hydrogen produced is able to react with the methane to produce methyl radicals which can then adsorb onto the substrate surface and initiate diamond growth.<sup>27</sup> Although methane gas is commonly used for the source of carbon, one study used a solid cylindrical graphite rod. With the tungsten breaking down the graphite rod producing atomic hydrogen and gaseous hydrocarbon species. This is an example of a closed system CVD method, the results showed the quality of the diamond improved, with a larger spacing between the graphite rod and the filament. This study concluded that the use of closed system CVD was safer due to less discharge of hydrogen into the atmosphere whilst also being more economically viable.<sup>28</sup>

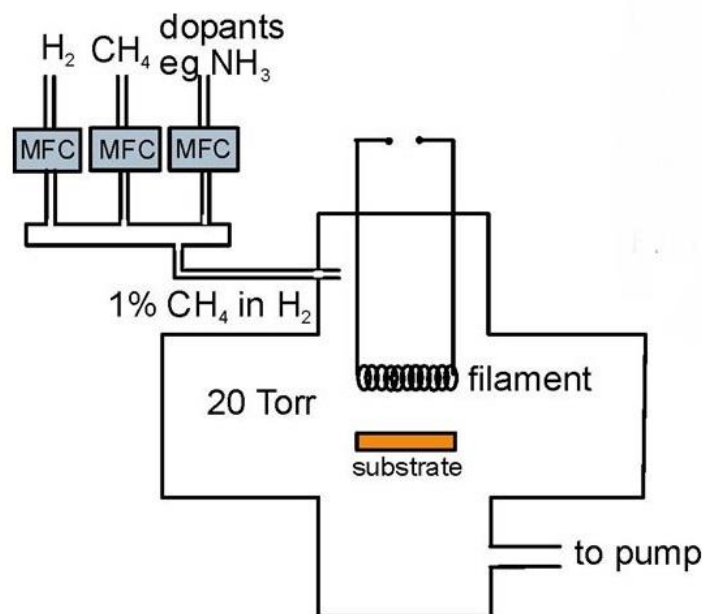
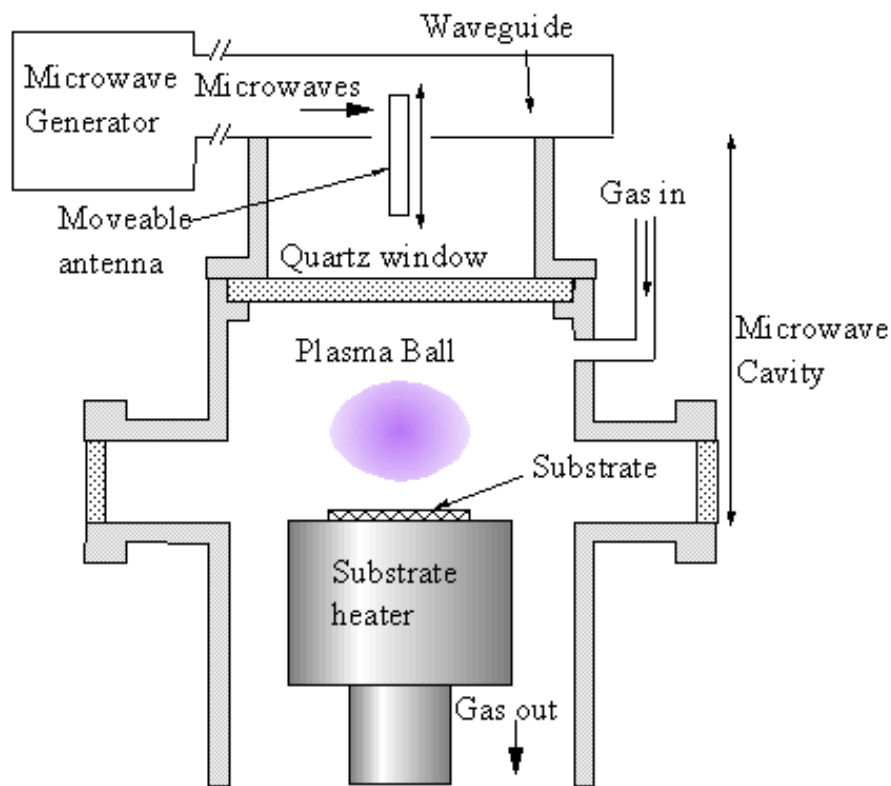


Figure 5 Diagram of a hot filament reactor and its components.<sup>29</sup>

One limitation of this method is where the tungsten filament absorbs some of the carbon when the precursor gas has been activated. This process is carburization and produces metal carbides which are brittle and results in filaments with relatively short lifetimes. This requires constant replacement of the filament, especially when long growth runs are conducted. Therefore, using a hot filament reactor could be cost inefficient. However, one study concluded that a carburized filament led to a higher nucleation rate for diamond hence more efficient growth of diamond thin films.<sup>30</sup> Another disadvantage of using this method is that a lower purity diamond is produced than other techniques due to metal contamination from evaporation of filament material. An advantage of a hot filament reactor is that large area of uniform diamond deposition is possible, reaching areas of 40 cm x 60 cm.<sup>31</sup>

### **Microwave Plasma CVD**

This method involves microwaves that activate the methane gas and dissociate molecular hydrogen to atomic hydrogen in the reactor chamber. Microwaves consist of perpendicular, oscillating electron and magnetic waves. As the microwave plasma oscillates electrons, they can collide with the feed gas resulting in ion production. Additionally, the electrons in the microwave dissociate molecular hydrogen. The presence of atomic and radical hydrogen species activate the carbon species, which can then be deposited onto the substrate. The density of the plasma and the energy of the electrons within are dependent on the frequency of the microwaves. 2.45 GHz is typically used for the frequency, providing a dense plasma with high energy electrons which results in more dissociation of molecular hydrogen hence faster growth rates.<sup>32</sup>



**Figure 6** Microwave Reactor and its components.<sup>33</sup>

The atomic hydrogen produced using microwave plasma assisted CVD has more kinetic energy than atomic hydrogen produced by a hot filament CVD. The result being much quicker growth rates. Another advantage of using microwave plasma CVD is that it requires no use of electrodes which ultimately provides higher purity of diamond due to lack of contamination.<sup>24</sup> One disadvantage of this technique is the limited deposition area where 2-3 cm substrates are usually used.<sup>32</sup> Although it is possible to scale up microwave plasmas it is very difficult. This is because to get even deposition and uniform diamond the substrate must be engulfed by the bottom of the plasma ball. To increase substrate size, plasma size must be increased greatly. To accommodate this chamber size must be increase greatly. Therefore, scalability is one limitation of a microwave reactor.

### Plasma-Jet CVD

This process works by creating a thermal plasma initiated between two electrodes, in a torch, connected to a direct current power supply and gas supply system. The gas supply is fed through a narrow gap into the chamber which has a cathode at the top. The gas is accelerated towards a torch nozzle and the anode. When the gas reaches the anode the DC arc discharge is formed and directed through the nozzle onto a water cooled substrate.<sup>34</sup>

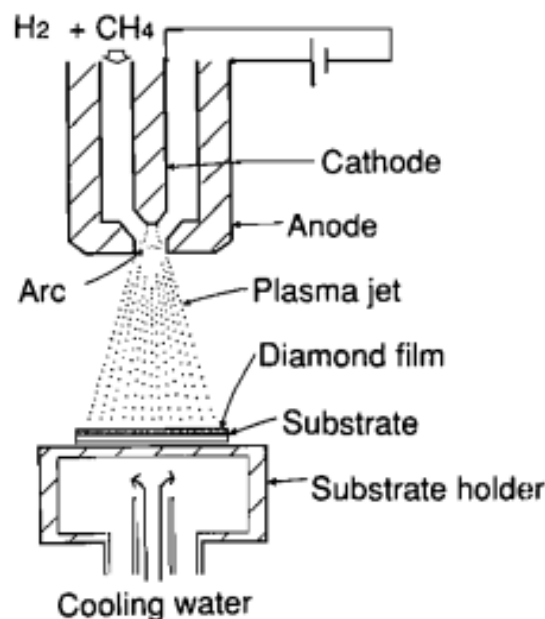


**Figure 7** Schematic diagram plasma-jet CVD reactor and its components.<sup>34</sup>

One advantage of this method is that it shows very high growth rates, as the high flow rate plasma is directly projected towards the substrate. As a result diamond deposition can occur at a reported  $200 \mu\text{m h}^{-1}$ .<sup>34</sup> Furthermore diamond can be deposited on relatively high substrate areas and provide a relatively high purity of diamond. The growth rate and the purity of the diamond is determined by the distance between the nozzle and the substrate. A study stated that for a distance of 5- 10 cm this gave a growth rate of  $6 \mu\text{m h}^{-1}$ . When increasing or decreasing the substrate-nozzle distance it was seen that the

growth rate decreased. Increasing this distance also saw the purity of the diamond deteriorate.<sup>35</sup> Furthermore, studies have shown that the growth rate and average diamond grain size increased when the input power of the plasma jet was increased.<sup>36</sup> It has been shown that using this method, large area and uniform diamond wafers can be grown. With values of 60-110 mm in diameter and 2mm in thickness, operating with a gas recycling mode.<sup>37</sup>

### **Pulsed DC Plasma Assisted CVD Reactor (PDR)**

The focus of the research in this project is centred on the PDR. This method works by creating a plasma between two electrodes. When a voltage is applied between the electrodes, electrons within the feed gas are accelerated towards the anode. As a result, positive ions of the gas mixture are formed and accelerate towards the anode and collide with it. Electrons are then released from the anode and pass through the gas mixture in the centre of the chamber. Collisions of the electrons with the gas causes ionisation by electron impact and this creates ions, atoms and radicals of the precursor gases, called a glow discharge.

As gas is fed into the chamber and is activated by the plasma, this allows the hydrocarbon radicals to deposit onto the substrate surface and initiate diamond growth. This method can provide high growth rates, comparable to the DC-arc jet plasma systems. With growth rates reported that values of up to 250  $\mu\text{m h}^{-1}$  are achievable.<sup>1</sup> Pulsed DC is used instead of continuous DC because this reduces the possibility of arcing. Arcing occurs due to a combination of high temperature at the cathode, where the electrode surface temperature causes thermionic emission processes to transition the plasma discharge from a glow to an arc, and the sputtering of hot carbonaceous material from the cathode by ion-bombardment which seeds an arc. Using a pulsed power supply employing arc suppression electronics cuts the power and prevents an arc.

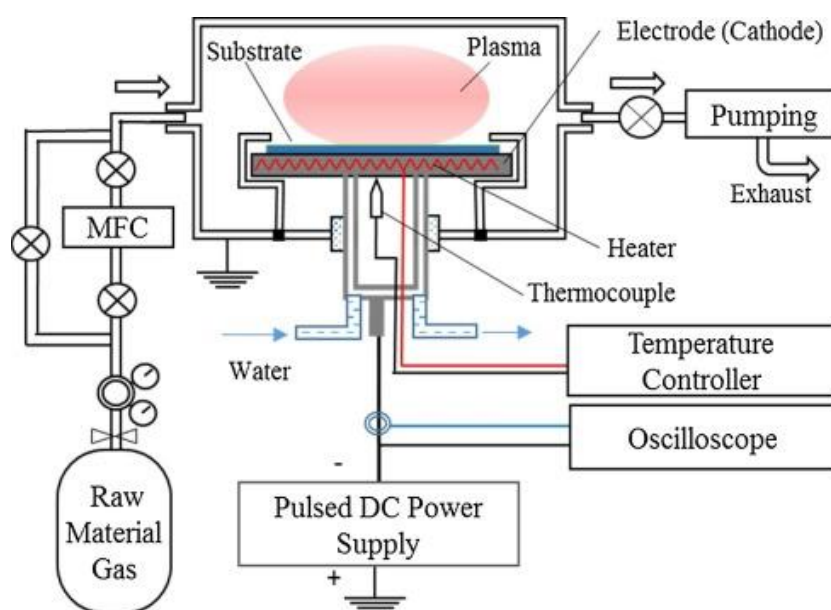


**Figure 8** Schematic diagram of a pulsed DC deposition reactor.<sup>38</sup>

Previous research has shown the possibility of growing large area diamond films with good quality at high growth rates. In terms of the pressure, 1 mm thick and 10 cm diameter diamond wafers were grown at 150 Torr.<sup>39</sup>

Having evaluated the techniques for CVD, it can be argued that the PDR may be the best method for growing diamond. This is because each of the other techniques had some major limitation such as limited growth rates or poor centre-to-edge growth uniformity.

### 3.4 Project Context

During this project, the construction of a mini-PDR has been undertaken. This mini-PDR will, after commissioning in the Diamond Lab, be transferred to the UK Atomic Energy Authority (UKAEA) for deployment in the interim H3AT facility. The purpose of this PDR is that it can be small enough to fit inside a fumehood system, which allows the safe handling of dangerous gases. UKAEA intend to use this to grow carbon-14 diamond using C-14 methane. The advantage of using this micro-reactor is that only a small volume of feedstock is required to accomplish active diamond growth which greatly lowers the safety concerns associated with active diamond growth.

The overall goal is to demonstrate incorporation of carbon-14 diamond into a battery. A nuclear battery with carbon-14 will have a stable output beyond the service life of most electronic devices with carbon-14 having a half-life of approximately 5,730 years.<sup>40</sup> Therefore, the creation of a beta-voltaic battery would be able to power devices with a small current for many decades or even centuries without need of replacement.

The UKAEA project is to synthesise single crystal diamond on iridium coated Yttrium Stabilised Zirconium (YSZ) substrates in a zero gas flow environment. In order to do so we must choose the best CVD method and optimise parameters with this method. As discussed, the pulsed DC plasma assisted CVD technique will be used.

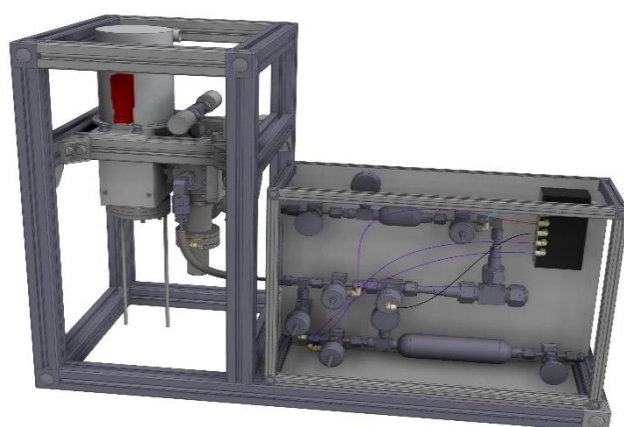


**Figure 9** CAD drawing of the mini-PDR provided by Dr James Smith at the University of Bristol.

### 3.5 PDR

The uniqueness of the PDR is connected with the growth taking place on a powered substrate/electrode combination, allowing higher rates of atomic hydrogen and electron current to impinge on the growth surface. When coupled with multi kilowatt levels of power that are available with the plasma power supply, this allows the conditions for nucleation and growth on challenging substrates such as copper alloys and single crystal substrates, such as iridium, to be accomplished. The parameters are: electrode separation, pressure, gas composition, temperature, power and pulse frequency. Looking at the literature, we can obtain optimum values for these. Literature experimental values will be inconsistent with our results as different substrates were used and experiments were done under continuous flow. However, these values will provide a basis from which an optimisation method can be used. By forming a processing window the best parameter values can be obtained.

#### Electrode Separation

The distance between the anode and the cathode is important in determining the crystalline quality of the diamond film. Noda et al.<sup>41</sup> claim that increasing the electrode distance from 10 to 20 mm provided the best quality films. Furthermore, for separations higher than this a sub electrode must be put near to the cathode. The result showing optimum crystalline quality between 20 to 25 mm.<sup>41</sup> However, without the use of a sub electrode, separations greater than 20 mm will result in the plasma becoming unstable. Other studies that have taken place at separations of 25-30 mm conclude that the diamond quality is essentially constant in this region.<sup>42</sup> Additionally Rai et al.<sup>43</sup> worked at electrode separations of 25 mm.<sup>43</sup> Larger electrode separations increase the electric field in the plasma ball. This helps mitigate the cathode over temperature.



Figure 10 The PDR reactor in the University of Bristol Diamond Lab.

## **Power and Frequency**

Pulses with higher power ultimately provide better deposition rates and a more efficient process. Higher plasma density shows higher degrees of ionization of the precursor gases.<sup>44</sup> As a result, there is a more efficient use of the precursor gases. This could be vital in closed gas cycle methods or where very limited amounts of source material are used. Rai et al.<sup>43</sup> found higher power values provided better deposition rates, with 306 Watts being the highest power value they used. Additionally, varying pulse rate frequencies from 0 to 200 KHz.<sup>43</sup> However, these measurements were conducted at  $7.5 \times 10^{-7}$  Torr. Lee et al.<sup>39</sup> had taken measurements at 150 Torr using input powers of 40 kW and 15  $\mu$ s between pulses provided growth rates of  $11 \mu\text{m h}^{-1}$ . Furthermore, the study concluded that increasing electric power provided an increased deposition rate, growth area and better crystal quality.<sup>39</sup> The frequency used in the diamond lab is 125 kHz so this would be a sensible starting point.

## **Gas Composition**

The composition of precursor gases is important as it determines the quality and growth rates during diamond deposition. Reshi et al.<sup>45</sup> concluded that the methane concentration in the precursor gas mix increases growth rate, nucleation and grain sizes of diamond. However, this was in a microwave plasma study conducted at a lower pressure and power level.<sup>45</sup> Haubner et al.<sup>1</sup> found that a lower methane concentration of 0.5 % provided better quality diamond facets. Furthermore, Haubner et al.<sup>1</sup> varied methane concentration from 0.5 % to 7 %. Growth rates of  $20 \mu\text{m h}^{-1}$  at 2 % methane concentration were recorded. Additionally, at an input power of 3.5 kW, growth rates of  $40 \mu\text{m h}^{-1}$  were obtained using 4 % methane. However, they found that the quality of the diamond films had decreased greatly as methane concentration increased, with quality determined by the amount of non-diamond carbon deposited.<sup>1</sup> In terms of argon concentrations, experiments conducted by Khamesh et al.<sup>46</sup> used 4:1 methane to argon ratios respectively.<sup>46</sup>

## **Pressure**

Most studies have conducted their research growth runs at 150-200 Torr. Haubner et al.<sup>1</sup> worked at pressures of 200 Torr in their varied methane concentration experiments. Raman spectra of deposition on stainless steel substrates indicated that higher deposition pressure led to more  $\text{sp}^2$  being present. However, these studies were conducted at 0.3 and 0.15 Torr.<sup>46</sup> Furthermore, Lee et al.<sup>39</sup> provided growth rates of  $11 \mu\text{m h}^{-1}$  whilst working at 150 Torr. Their method was to strike the plasma at 1 Torr and to slowly raise the pressure.<sup>39</sup> The higher the pressure, the higher the production of atomic hydrogen. As many diamond growth studies using pulsed-DC plasma use pressures between 150 and 200 Torr, 180 Torr would be a sensible pressure to begin with. This is because 180 Torr provides a high pressure to efficiently produce atomic hydrogen, necessary for diamond growth.

### **3.6 Single Crystal Growth**

Single crystal diamond growth is researched because of its many potential applications. Many applications require films of very high crystalline quality, where polycrystalline diamond will not suffice, such as power switching transistors and radiation detectors.<sup>47</sup> Polycrystalline films have too many structural defects which can lead to degradation of some properties which would overall cause a device to perform poorer than expected.<sup>48</sup> For example, structural defects prevent diamond containing electronic devices to suffer as there is drastically reduced charge carrier mobility.<sup>49</sup> Furthermore, Linares et al.<sup>48</sup> claim the presence of defects and impurities can degrade the mechanical and optical

properties of diamond.<sup>50</sup> More examples of uses of single crystal diamond are in systems that require quantum photonics, quantum computing and magnetometry.<sup>48</sup>

Shikata et al.<sup>47</sup> discussed single crystal diamond and its potential in CO<sub>2</sub> reduction. The International Energy Agency proposed the use of low loss power devices as being an integral technology for CO<sub>2</sub> reduction. IEA want 25 % CO<sub>2</sub> reduction from 'end use efficiency', which describes getting more usage from a device per unit energy consumed. Diamond's excellent electronic properties such as its high mobility and low dielectric constant make it a favourable candidate for low loss power device modules. Shikata explains that the expected application of diamond here is to provide high voltage and high output power devices.<sup>47</sup> Single crystal diamond would be necessary for these devices as minimal structural defects would be required for a low loss power device.

Much research has gone into the growth mechanisms of single crystal diamond. Single crystal diamond can be grown homoepitaxially or heteroepitaxially. Homoepitaxial growths requires the substrate and growth layers to be the same material whilst heteroepitaxial growth requires them to be different. Homoepitaxial growth provides better quality diamond films by having less dislocation densities than heteroepitaxial films. With homoepitaxial films having between 10<sup>3</sup> and 10<sup>7</sup> dislocations cm<sup>-2</sup> and heteroepitaxial films having between 10<sup>7</sup> and 10<sup>10</sup> dislocations cm<sup>-2</sup>.<sup>48</sup> However, heteroepitaxial films can be grown in much larger areas. Being able to grow larger area films would be more cost and energy efficient.

If carbon-14 diamond batteries were constructed, single crystal diamond must be used. This is because single crystal diamond contains fewer defects and grain boundaries, hence enhanced charge carrier mobility.

### **YSZ Iridium Substrates**

Iridium is often used in research of heteroepitaxial single crystal growth of diamond. For successful heteroepitaxial growth crystal structure and lattice parameters must match. Furthermore, growth on foreign substrates require nucleation of a precursor gas.<sup>49</sup> Arnault et al.<sup>48</sup> claim iridium substrates provide diamond films with the best crystalline quality.<sup>48</sup> The crystallinity match of iridium for diamond is an order of magnitude better than other substrates such as silicon, platinum, palladium and nickel.<sup>51</sup>

Verstraete et al.<sup>51</sup> found iridium substrates highly favoured carbon dissolution into the bulk. Additionally, they found iridium as the only substrate which could expel enough carbon to the surface at an efficient enough rate for effective diamond nucleation and growth.<sup>51</sup>

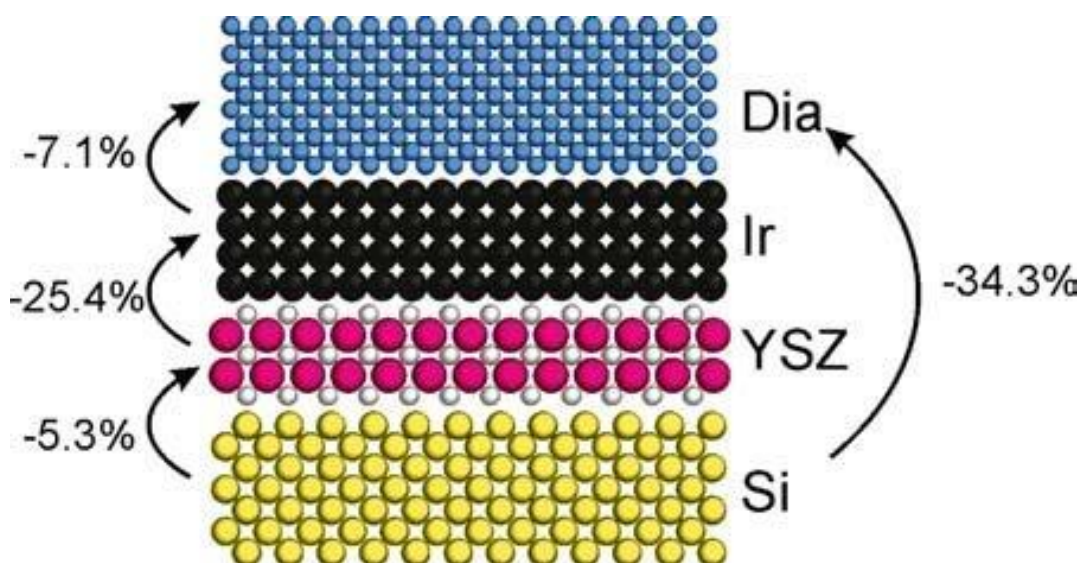


**Figure 11** Layered structure of diamond growing on layered Si/YSZ/Ir. Percentages show difference between lattices for each layer.<sup>52</sup>

The reason iridium is placed on coated Yttrium Stabilised Zirconium (YSZ) is because having pure iridium substrates would be very costly. Furthermore, iridium is difficult to resource due to its lack of availability. A study from Gsell et al.<sup>52</sup> saw the use of iridium YSZ buffer layers on silicon. These were constructed by pulsed-laser deposition of a YSZ layer on silicon followed by electron beam evaporation to deposit the iridium. XRD data showed how YSZ formed a perfect buffer layer for the growth of iridium on silicon. Mosaicity of the diamond films were achieved at an order of magnitude higher with the iridium YSZ buffer layers than without.<sup>52</sup>

### **3.7 Static Flow**

Traditional CVD uses a continuous flow of the precursor gases. On the PDR, to do continuous flow, a combination of mass-flow controllers and a butterfly valve allow a constant pressure to be obtained in the chamber. Static flow involves adding the precursor gases to the required pressure, then closing the gas flows and vacuum pump. Studies conducted on ‘static-flow’ CVD have shown that diamond can be grown to the same quality as using continuous flow. Croot et al.<sup>5</sup> found that diamond grown in static-mode and continuous flow were very similar in diamond quality and crystalline morphology. Furthermore, they found using static flow techniques offered a 30-fold improvement in the efficiency of the conversion of carbon from the precursor gas mixture. These studies were carried out using microwave plasma CVD.<sup>5</sup>

To design a diamond battery, static flow conditions would be necessary. Carbon-14 is a highly radioactive material, using as low amounts as possible in diamond synthesis would be a safer and more sensible practice. Furthermore, carbon-14 is harder to source than carbon-12 or carbon-13 and is more expensive. Therefore, using static-flow CVD provides a more economically viable option as well as a safer option.

### **3.8 Characterisation**

In order to characterise the discharge plasma and the samples grown optical emission spectroscopy, Raman spectroscopy and scanning electron microscopy will be used.

### 3.8.1 Optical Emission Spectroscopy (OES)

OES provides the elemental breakdown of the species in the glow discharge plasma. OES measures the emission intensity of each emitting species in the plasma, based on the discrete wavelength of light each specie emits. Species emit wavelengths of light from electron de-excitation. The emitting species are generally formed by electron impact excitation within the plasma. Within a CH<sub>4</sub>/H<sub>2</sub> mixture, OES provide information on Balmer series of H atoms, CH and C<sub>2</sub> radicals. If argon was incorporated into the gas mixture excited Ar atoms would also be present and seen in the spectrum.<sup>53</sup>

**Table 2** Optical emission spectroscopy characteristics for a CH<sub>4</sub>/H<sub>2</sub> plasma.<sup>54</sup>

<u>Species</u>	<u>Wavelength/ nm</u>	<u>Upper Level</u>	<u>Lower Level</u>	<u>Energy Difference/ eV</u>
CH	431.1	A <sup>2</sup> Δ	X <sup>2</sup> Π	2.88
H <sub>β</sub> (Balmer-β emission)	486.1	n=4	n=2	2.55
C <sub>2</sub>	516.5	d <sup>3</sup> Π <sub>g</sub>	a <sup>3</sup> Π <sub>u</sub>	2.32
H <sub>2</sub>	602.1	3p <sup>2</sup> Σ <sup>+</sup> <sub>u</sub>	2s <sup>3</sup> Σ <sup>+</sup> <sub>g</sub>	1.44
H <sub>α</sub> (Balmer-α emission)	656.3	n=3	n=2	1.9
Ar (4p)	750.4	3s <sup>2</sup> 3p <sup>5</sup> [ <sup>2</sup> P <sup>o</sup> <sub>1/2</sub> ]4p	3s <sup>2</sup> 3p <sup>5</sup> [ <sup>2</sup> P <sup>o</sup> <sub>1/2</sub> ]4s	1.66

Furthermore, CN and N<sub>2</sub> species may be seen in the spectrum, this would be indicative of impurities within the gas mixture. This could be due to air contamination within the chamber. Bulou et al.<sup>55</sup> reported CN peaks at 388.3 nm that correspond to the B<sup>2</sup>Σ to X<sup>2</sup>Σ transition.<sup>55</sup>

One advantage of using optical emission spectroscopy is that it provides information on intensities within the plasma without disturbing it.<sup>56</sup> However, one disadvantage of using OES is that it can only be used to monitor species that happen to emit in the visible wavelengths.

### 3.8.2 Raman Spectroscopy

Raman spectroscopy can characterise a sample using scattered light, measuring the energy of photons before and after they've been scattered. When light interacts with a material, the photons can interact elastically or inelastically. An elastic collision results in no energy transfer between the incident photon and the electron, this is known as Rayleigh scattering.

An inelastic collision does involve an energy transfer. If the photon has higher energy after scattering, the electron within the sample must have lost energy, this is Anti-stokes scattering. However, if the photon has lower energy after interacting with the sample, the electron would have gained energy, this is Stokes scattering.<sup>57</sup>

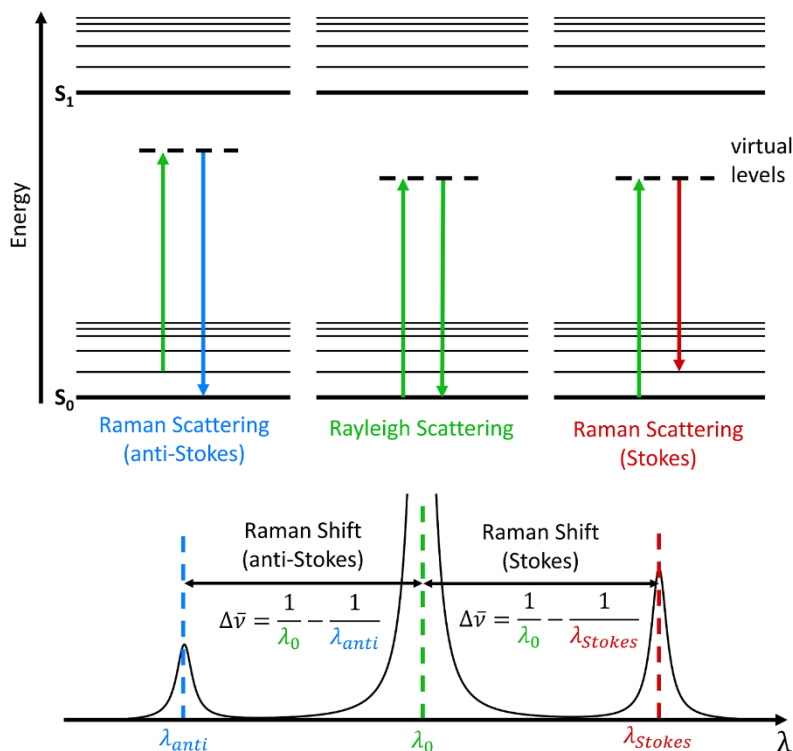


Figure 12 Diagram showing the change in wavelengths for Raman scattering.<sup>57</sup>

Each of these provide information on the discrete vibrational energy levels of a sample. Therefore, a sample can be characterised using Raman spectroscopy by measuring their vibrational energy modes. Peaks at  $1332\text{ cm}^{-1}$  are indicative of diamond material. Table 3 shows that there are 2 peaks for  $\text{sp}^2$  carbon, the D peak at  $1345\text{ cm}^{-1}$  and the G peak at  $1520\text{-}1580\text{ cm}^{-1}$ . The D peak refers to disordered  $\text{sp}^2$  carbon and the G peak refers to crystalline  $\text{sp}^2$  carbon. The presence of  $\text{sp}^2$  carbon peaks is unwanted as this indicates impurity within the diamond.<sup>58</sup>

Table 3 Raman characteristics of CVD diamond and some of its impurities.<sup>59</sup>

Wavenumber Shift/ $\text{cm}^{-1}$	Assignment
1332	First-order Raman line
1345	$\text{Sp}^2$ amorphous carbon (the D peak)
1520-1580	$\text{Sp}^2$ crystalline carbon (the G peak)

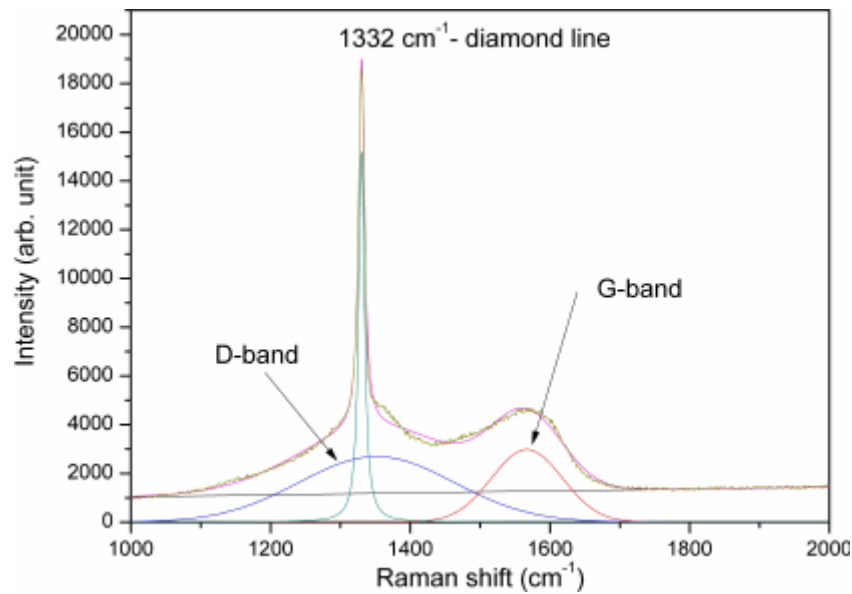


Figure 13 Raman spectrum showing diamond and amorphous carbon peaks.<sup>60</sup>

### 3.8.3 Scanning Electron Microscopy (SEM)

Scanning electron microscopy (SEM) is commonly used to characterise micro and nanoparticles of solid objects. SEM instruments have an electron gun which emits electron beams that are accelerated with high voltages, typically 20 kV.<sup>61</sup> Electromagnetic lenses are then used to focus the beam on a small section on surface of the analyte. The analyte surface is scanned with the electron beam.

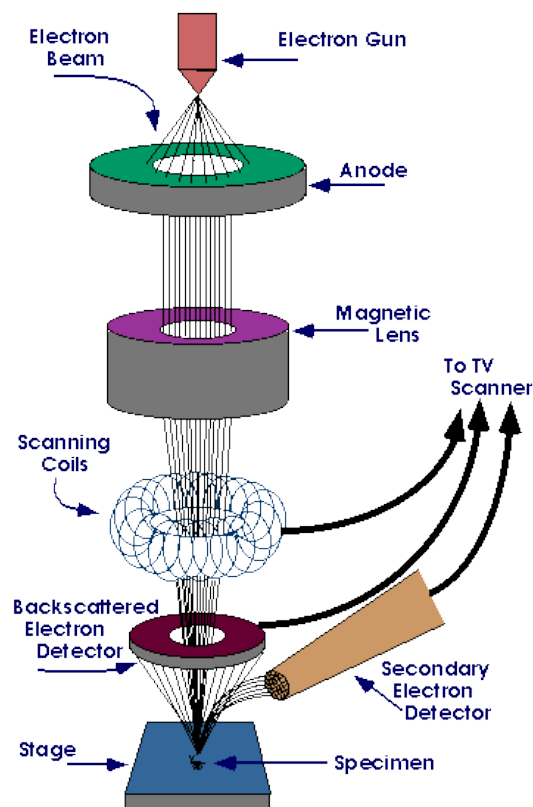
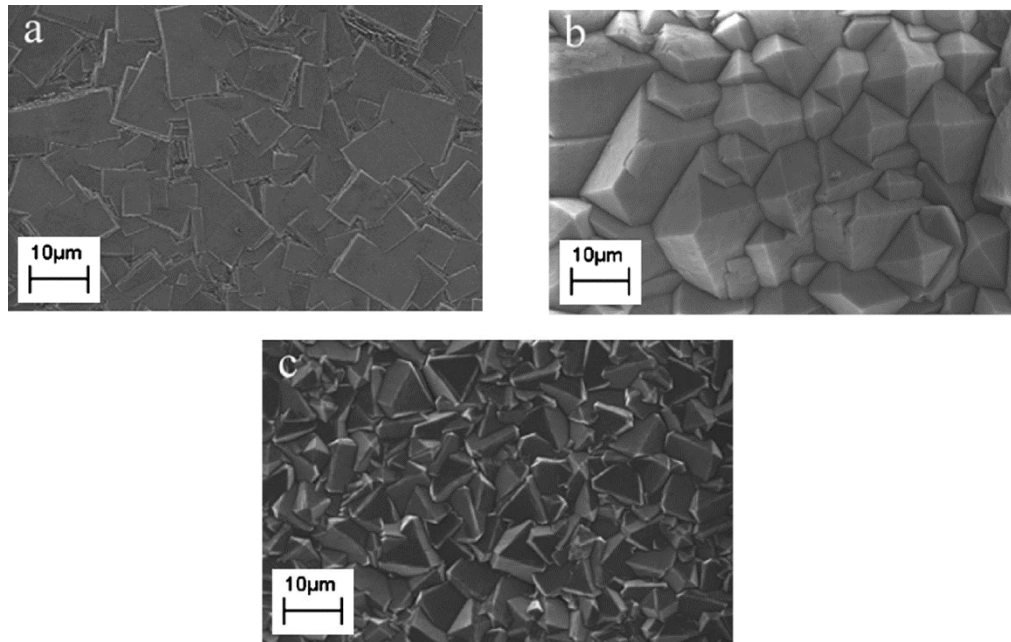


Figure 14 Schematic diagram of a scanning electron microscope.<sup>62</sup>

The interactions of the electrons and the sample surface produce signals that are collected by a detector. Images of the scanned area of analyte are then generated based on the signals measured. Electrons can be scattered and absorbed by air and so a high vacuum system is necessary for accurate images.<sup>61, 63</sup>



**Figure 15** SEM images of polycrystalline diamond. Textures: a) 100 b) 111 c) 110. The diamonds were grown using a DC discharge plasma enhanced system. Grown on single-crystal 450  $\mu\text{m}$  thick Si (100) chips of 25 $\times$ 25 mm. Using a variation between 3 to 6 % methane.<sup>64</sup>

One advantage of SEM techniques is that they provide high levels of precision, giving resolutions as precise as 10 nm.<sup>61</sup> Another advantage of using SEM instruments is the versatility of information provided. Three-dimensional images are produced providing topographical and morphological information that is collected using a variety of detectors.<sup>65</sup> Different modes of SEM include backscattered imaging and secondary electrons imaging.<sup>65</sup> However, disadvantages of using SEM is that the instruments are expensive, large and require much maintenance.

### **3.9 Taguchi Method**

The Taguchi method is an efficient optimisation method that can be used to find the best parameters for diamond growth. This method takes into account three factors: noise, signal and control. Noise factors describe parameters that are uncontrollable and affect the outcome of a product. Control factors are independent variables and are the input parameters for the experiment, for diamond CVD they would be factors such as methane concentration and power. Signal factors reflect the quality of a product, for diamond CVD they are crystallinity, purity, and growth rate. The Taguchi method aims to minimise the number of experiments necessary to find the best choice of control factors that provide the best quality output.

The control factors for the experiment must be determined. Each control factor should then be split into at least two different levels, providing a range for each control factor. With the number of control factors determined and levels given for each one, an orthogonal array is produced. An example of an orthogonal

array with 4 control factors with 3 levels each is shown in **table 4**. A signal-to-noise ratio is calculated for each level and parameter from the experiments in the orthogonal array and tabulated. The range of the signal to noise ratio for each control factor is calculated, the parameters with the biggest range have the biggest effect on the signal factors.

**Table 4** Example orthogonal array of 4 parameters and 3 levels each. This shows the number of experiments necessary.

<b>Experiment No.</b>	<b>Parameter 1</b>	<b>Parameter 2</b>	<b>Parameter 3</b>	<b>Parameter 4</b>
<b>1</b>	1	1	1	1
<b>2</b>	1	2	2	2
<b>3</b>	1	3	3	3
<b>4</b>	2	1	2	3
<b>5</b>	2	2	3	1
<b>6</b>	2	3	1	2
<b>7</b>	3	1	3	2
<b>8</b>	3	2	1	3
<b>9</b>	3	3	2	1

## 4 Experimental Method

### 4.1 Experiments and Aims

The introduction and literature review from section 3 was for a previous project that was abandoned due to equipment failure.

The aim of this research was to see which method would provide us with the best quality diamond grown with different static flow cycles. To do so methane concentration and chamber conditions will be varied. Chamber conditions were varied in terms of boron-doping: one chamber being completely undoped and one residually boron doped. For methane concentration, 4 % and 6 % methane in hydrogen will be varied. For each of these conditions five growth runs will be tested: a continuous flow run and four static cycles. The static cycles to be tested reintroduce methane and hydrogen every 120, 60, 40 and 30 minutes. Every single run is two hours long. The growth rates, purity and crystallinity are determined for each growth.

**Table 5** Outline of all the experiments conducted. Table showing methane percentages for each reactor condition.

	<u>Interval</u> <u>Time/min</u>	<u>Residually Boron Doped (R)</u>		<u>Undoped (U)</u>	
<b>F120</b>	<b>Continuous</b>	<b>4%</b>	<b>6%</b>	<b>4%</b>	<b>6%</b>
<b>ST120</b>	<b>-</b>	<b>4%</b>	<b>6%</b>	<b>4%</b>	<b>6%</b>
<b>ST60</b>	<b>60</b>	<b>4%</b>	<b>6%</b>	<b>4%</b>	<b>6%</b>
<b>ST40</b>	<b>40</b>	<b>4%</b>	<b>6%</b>	<b>4%</b>	<b>6%</b>
<b>ST30</b>	<b>30</b>	<b>4%</b>	<b>6%</b>	<b>4%</b>	<b>6%</b>

### 4.2 Seeding

The substrates used for each of our growth runs were 10 x 10 mm silicon squares. Before any growth was conducted these substrates were seeded to provide nucleation points on the substrate for successful diamond growth. The samples were seeded using electrospray ionisation with a nanodiamond solution suspended in methanol. The solution was first sonicated for 60 minutes to break up any nanodiamond aggregates present. The solution is then sprayed onto a rotating metal disc holding six of the silicon squares. The solution is aimed at the disc using a potential difference. The box encasing the spray nozzle and the nozzle itself have a voltage of 65 kV and the rotating board is grounded. The charged droplets from the nanodiamond solution are accelerated towards the grounded disc, seeding nanodiamonds onto the silicon substrates.

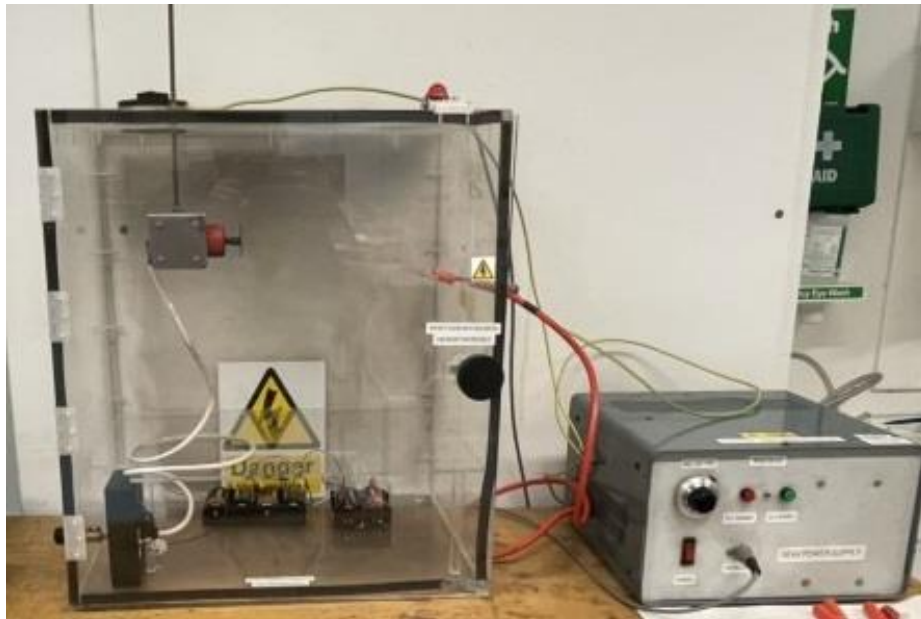


**Figure 16** Electro spray kit used for seeding.

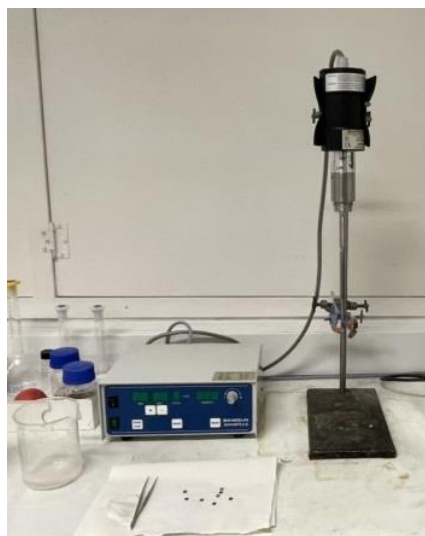


**Figure 17** Sonicator used to break up diamond aggregate solution used for seeding.

### **4.3 Reactor Design**

A microwave reactor was used to conduct each growth run. An exhaust valve controller controls the vacuum pump and butterfly valve, necessary to determine pressure within the chamber. The butterfly valve effects how much gas is pumped away depending on the extent it is open. To determine the rate of gas flow into the chamber mass flow controllers were used. This allowed the methane concentration to be kept constant. A pyrometer was used to measure the temperature of the substrate within the reactor. Chilled water is used to cool the chamber, water flows are monitored using a flowmeter below the reactor. An air blower is used for air cooling in the chamber.

All these features were incorporated into the undoped and the boron residually-doped chambers. However, the residually boron doped chamber had an extra pipe which connects the vacuum pump to the chamber. This was to reduce exposure of the diborane to air, with the pipe having a substantial area. To keep the substrate at an adequate temperature, a 4 milli-inches spacer was used to reduce the amount of water cooling to the substrate. Each reactor had gas lines feeding directly into the chamber. For the residually-doped growths the diborane line was important to residually dope the chamber. The undoped chamber has a methane gas tap to allow flow into the chamber whilst the residual chamber did not. Both reactors had a tap that connects all the gas lines to the chamber, the chamber tap. Each reactor chamber had an air inlet to allow the chamber to slowly reach atmospheric pressure, this must be closed whenever the pump is open, so air is not sucked into the pump. See **figure 6** for a schematic diagram of a microwave reactor.

#### **4.4 Reactor Operation**

Two different methods were used to start the growth runs, depending on whether continuous or static flow were conducted.

##### **4.4.1 Continuous Flow Start**

For every continuous flow run the following procedure was used. Once the substrate sample had been loaded, the chamber was pumped down, ideally to approximately 10 mTorr. For the residually-doped chamber, the tap that connects the pump to the chamber was opened. Once pumped down, the required gas taps were opened. The water chiller and air blower were turned on, water flow and air blowing through the chamber were then checked. Hydrogen was flowed at 300 sccm into the chamber and the pressure built to 15 Torr. At 15 Torr the microwave power was turned on at 700 W to strike a plasma and the position of the plasma on the substrate was immediately checked. The exhaust valve controller was set to 150 Torr and pressure was allowed to build. At 50 Torr, methane was flowed in (flow rate depending on desired concentration). At 70 Torr, the power was dialled to 1500 W, maintaining an approximate 10:1 ratio of pressure to power. Once pressure reached 150 Torr and power 1500 W, the two hour run began. Methane flow rates of 12 and 19.2 sccm for 4 % and 6 % concentrations, respectively were used.



**Figure 18** Undoped chamber used to conduct undoped runs.

#### **4.4.2 Static Flow Start**

Similar to continuous flow, once the sample is loaded, the chamber was pumped down to approximately 10 mTorr. For the residually-doped chamber, the tap that connects the pump to the chamber was opened. Again, the required gas taps were opened. The water chiller and air blower were turned on, water flow and air blowing through the chamber were then checked. Hydrogen was flowed at 300 sccm into the chamber and the pressure built to 15 Torr. Once 15 Torr has been reached, the microwave generator was turned on and a plasma struck at 700 W. The position of the plasma on the substrate was then checked. Immediately after, the pump was closed using the exhaust valve controller and methane was added. Once the pressure reached 70 Torr, the power was dialled up, maintaining an approximate 10:1 ratio. When the pressure reached 150 Torr all gas flows on the exhaust valve controller were turned off and the power tuned to 1500 W. To cycle in hydrogen and methane during this run, the exhaust valve controller to automatic was set to maintain pressure at 150 Torr. The gases were added for 30 seconds, then the flows closed immediately and the exhaust valve controller was set back to close.

#### **4.4.3 Shutting Down**

The shutting down procedure at the end of a run was very similar for continuous and static methods. For continuous flow, the methane flow was closed and hydrogen was flowed for two minutes. For static flow, the exhaust valve controller was set to automatic at 150 Torr. Then only the hydrogen flow was opened for two minutes. Following this, the power and pressure were dialled down, maintaining a 10:1 power to pressure ratio. Once 30 Torr is reached, the power was dialled to 0 W and the microwave generator was turned off. The vacuum pump was opened via the exhaust valve controller and all gas flows and gas taps were closed. Once the reactor had pumped down, the pump was closed and the air inlet was slowly opened to allow the chamber to reach atmospheric pressure (approximately 760 Torr). For the residually-doped reactor the tap connecting the pump to the chamber was closed before the air inlet was opened.

#### **4.5 Residual Doping**

To keep results comparable, the level of residual doping must be kept approximately constant. To achieve this, before every residually-doped run a diborane/methane/hydrogen plasma was struck. The method to strike the plasma was the same as the continuous flow start up procedure however without a substrate. Make sure the diborane tap is open and when 50 Torr is reached and add diborane at the same time methane is added. Once 150 Torr is reached, the plasma stood for two minutes then the standard shut down procedure above was used. The diborane gas line was always the last tap opened and the first one closed to ensure a positive flow of hydrogen through the pipes.



**Figure 19** Residually boron doped chamber used to conduct residually boron doped runs.

#### **4.6 Test**

For every static flow cycle, the gases are flown in for 30 seconds. This time was determined after a 1 hour static test run. The standard static start up procedure was used and the growth monitored using OES. OES data from the start of the reaction was taken and the intensity of the  $C_2$  radical was recorded. An hour into the static run, the OES program was set to save spectra every 0.25 s. A precise time taken to refill the methane to the initial  $C_2$  intensity was found. The results from this test show that it takes at least 30 seconds to stably reach the initial  $C_2$  concentration.

### **5 Characterisation**

#### **5.1 OES**

The program Waves was used for all optical emission spectroscopy analysis. A Broadcom Qmini spectrometer was used connected to a lens via a fibre optic cable. For each run, spectra were taken every 0.5 minutes. The residually boron doped chamber had clean optical windows at the side, suitable to conduct OES with. However, the undoped chamber had dirtier windows, meaning the OES lens looked through the top of the chamber. A graph of the  $C_2$  swan band at 516.4146 nm against time is plotted for each run. This provides an indication and monitor of the concentration of carbon species in the plasma. For each data set, growth runs were plotted having been normalised, offset and baseline corrected. They were normalised to the highest  $C_2$  concentration value during the run. This gave a clear way to compare each growth within a data set.



**Figure 20** Optical emission spectrometer used in this research.

## **5.2 Raman Spectroscopy**

Raman analysis provides information on the quality of a sample including purity and crystallinity. The peak at  $1332\text{ cm}^{-1}$  is indicative that diamond is present. Bands at approximately  $1500\text{ cm}^{-1}$  were inspected and show whether graphite is present. For each sample three spectra were taken, across the sample to show whether a sample was uniform. One spectrum per sample was analysed using baseline corrections and curve fitting. The value of the full width half maximum was then obtained for each sample. Furthermore, the data for each spectrum taken was exported to excel. For each data set the spectra were offset, baseline corrected and normalised, allowing us to compare each growth run clearly.



Figure 21 Raman spectroscopy kit.

### **5.3 Scanning Electron Microscopy**

SEM provided the thickness of each sample. Top view and cross-sectional images were taken at the edges and centres of each sample. Using paint software, the thickness of the cross-section was measured using the pixel count on the program. The images were at a  $70^\circ$  angle, therefore, to get the actual thickness of the sample, the measured thickness was multiplied by  $\sin(70)$ . Having calculated the thicknesses, growth rates were calculated. Using SEM, it is possible to see which conditions provided the quickest and slowest growth rates and information on the uniformity of the film was given.

## 6 Results and Discussion

### 6.1 OES

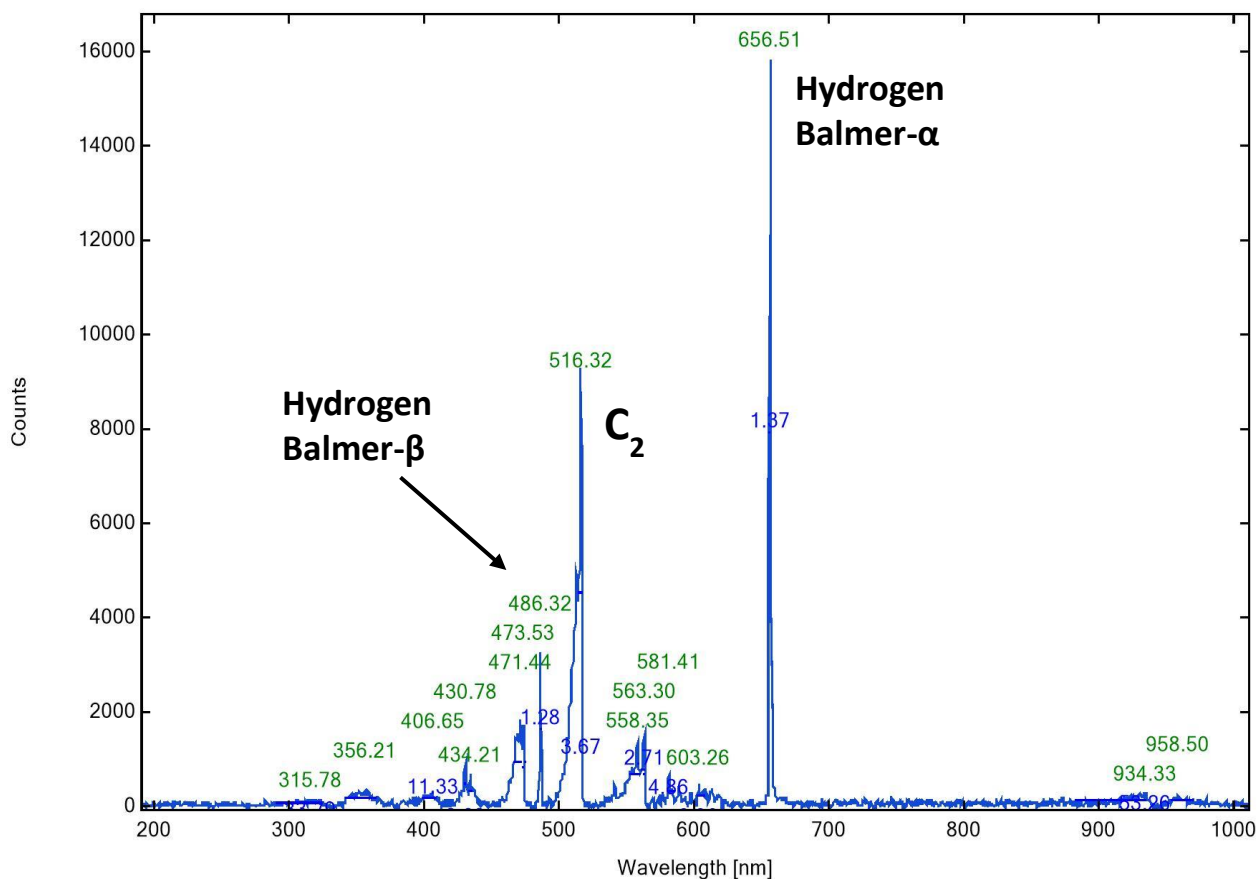


**Figure 22** An example optical emission spectrum taken from the residual 4 % flow run. Spectrum was taken 1 hour 40 minutes into the run.

The spectrum shown in **figure 22** was taken nearing the end of a flow run. The spectrum shows the hydrogen Balmer-  $\beta$  at 486.32 nm, the  $C_2$  peak at 516.32 nm and the hydrogen Balmer-  $\alpha$  peak at 656.51 nm. The important feature to look at for this run is the difference in intensity between the hydrogen Balmer-  $\alpha$  peak and the  $C_2$  peak. Each spectrum throughout this run looked very similar, this is expected because the methane and hydrogen are consistently being flown for the duration of this run. Hence the relative concentrations for them would remain constant.

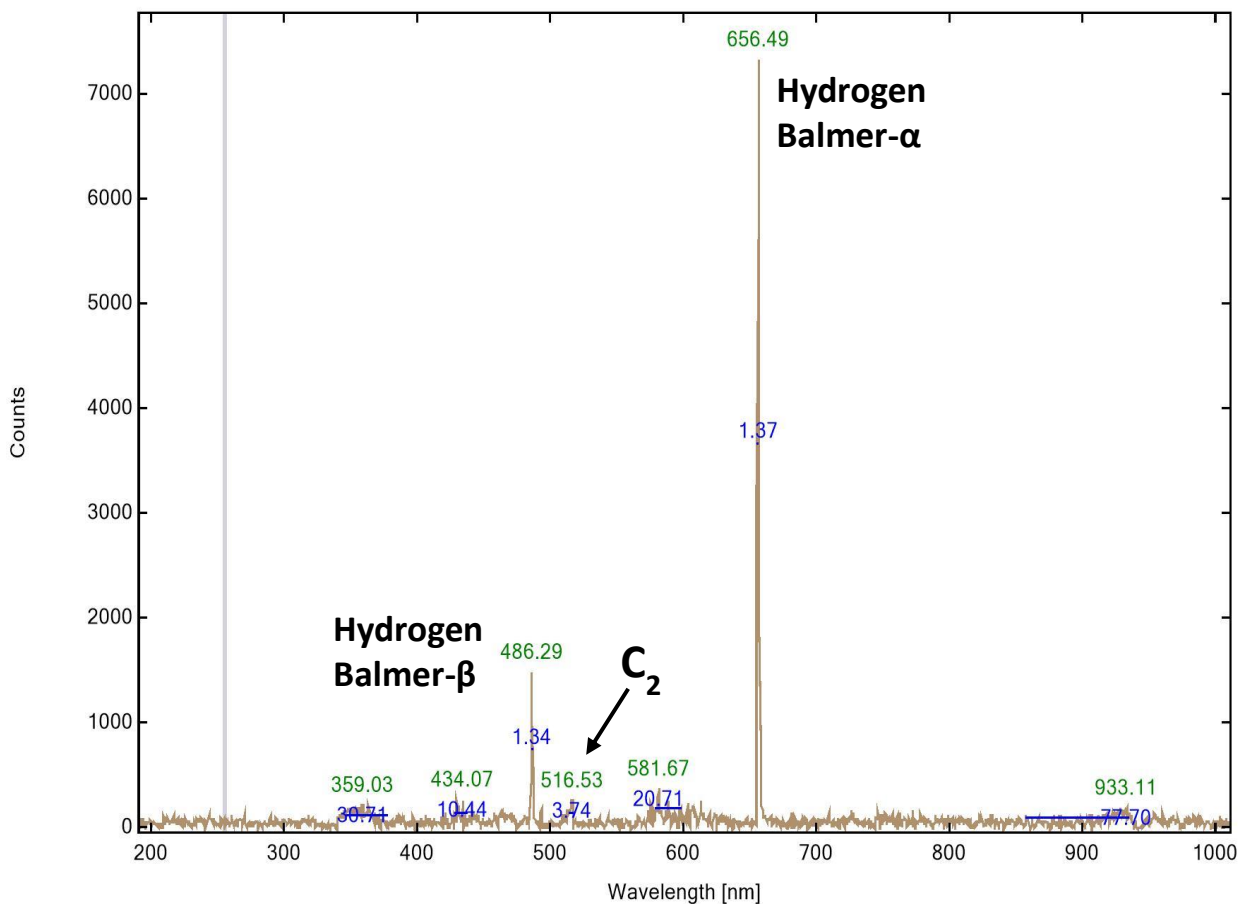


**Figure 23** An example optical emission spectrum taken from the residual 4 % ST120 run. Spectrum was taken 1 hour 40 minutes into the run.

This spectrum is taken from the same data set as the flow spectrum and at the same time in the run. The C<sub>2</sub> peak has diminished compared to the hydrogen- α peak. This is expected as the precursor gases were not introduced at any point during the run. As carbon species are being deposited, without reintroducing methane, the C<sub>2</sub> peak decreases as the run continues. During the static run the methane concentration starts high, providing a spectrum very similar to the flow spectrum in **figure 22**. However, during the run as methane decreases and the hydrogen concentration stays approximately constant and, a spectrum in **figure 23** is seen where the C<sub>2</sub> peak has essentially become part of the background noise.

### 6.1.1 Test

Using the results from the test discussed in the experimental, it was concluded that the precursor gases should be flown for 30 seconds.

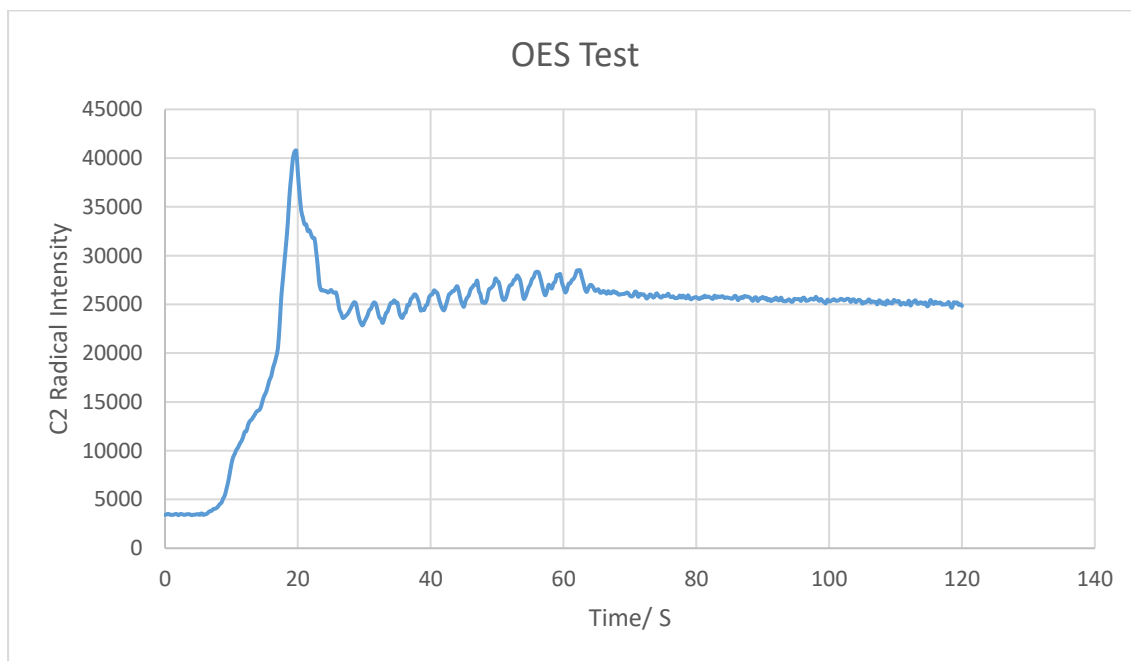


**Figure 24** OES test results to determine how long precursor gases should be flowed during static cycling.

As hydrogen and methane were introduced, a spike in intensity is seen at 20 seconds. This spike could be due to methane not having entered the chamber and residing in the gas lines during the run. If gases were flowed in for 30 seconds, the spike would be surpassed with the  $C_2$  intensity becoming stable. It was necessary to flow the gases in for as short as possible because static flow is designed to be conservative on gases.

### 6.1.2 4% and 6% Residually-Doped Data

The OES data from these two sets were analysed the same and provided very similar results. The point of showing this data was to show the depletion of methane by monitoring the  $C_2$  radical intensity. The  $C_2$  intensity is not a direct measurement of the methane concentration within the chamber however, it can be used as an indication.

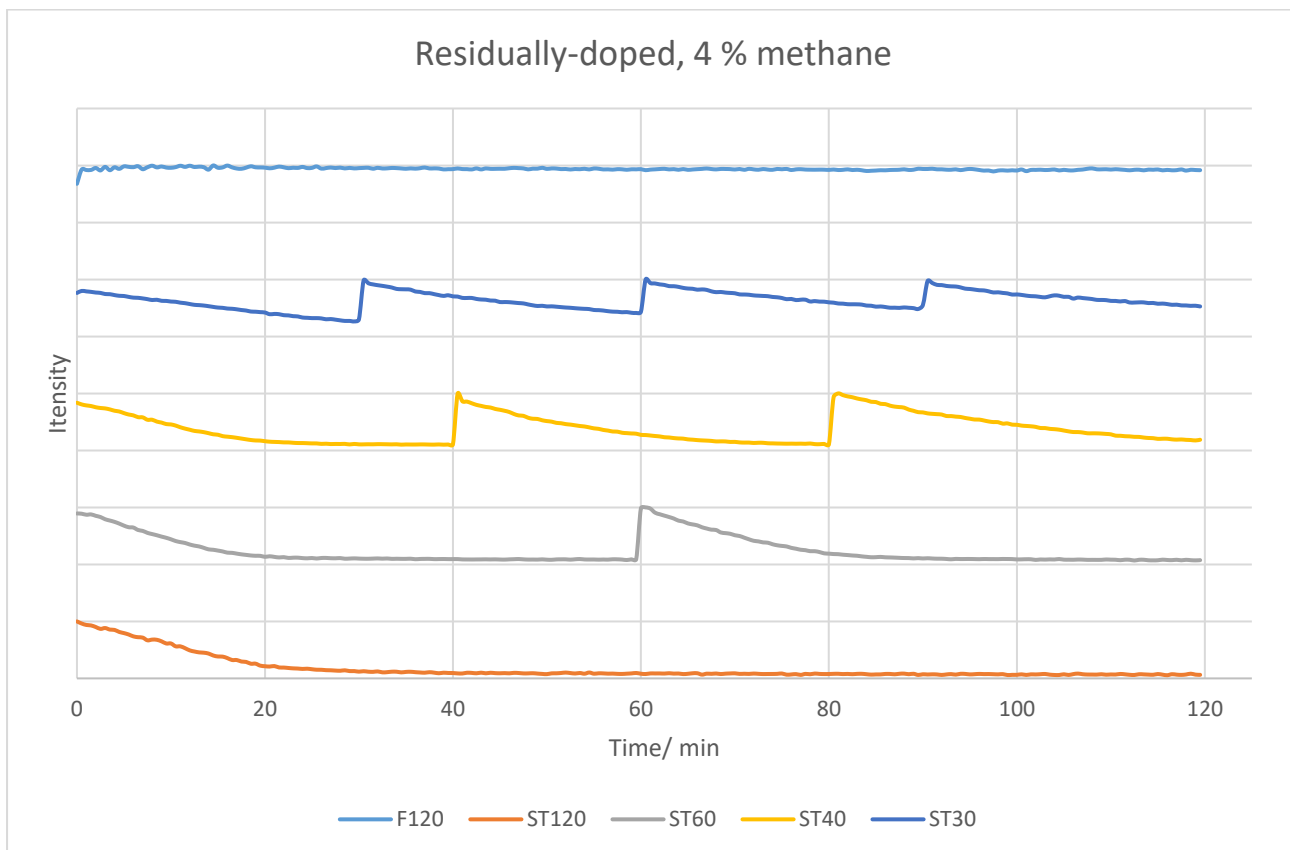


**Figure 25** OES results showing  $C_2$  concentration for the residually-doped 4 % data set.

For the residually-doped 4 % data set, throughout the continuous flow run the  $C_2$  concentration remains constant. This is expected as methane and hydrogen are constantly being flowed through the chamber for the duration of the run. The ST120 run shows the  $C_2$  concentration decreasing until approximately 20 minutes, after this the concentration plateaus. This suggests that the methane was mostly all used up during the first 20 minutes of the growth run. For the other static cycles, the concentrations plateau similar to the ST120 static cycle. However, when gases were cycled in, a sharp increase in the  $C_2$  concentration is seen, approximately to the same value as the initial concentration.

In some cases such as the refilling done at time= 40 min in the ST40 run, the concentration of  $C_2$  higher than at time= 0 min. One explanation for this could be because carbon that had been deposited onto the substrate would have desorbed back into the gas phase. The result being a higher concentration of  $C_2$  radicals than expected. This could also be visibly observed during gas cycling in the ST30 run. Overall, OES results show that the cycling of gas for the static runs was successful, reaching a concentration close to the initial for this data set. For the residually-doped chamber, the lens was directed at the middle of the plasma through an optical window.

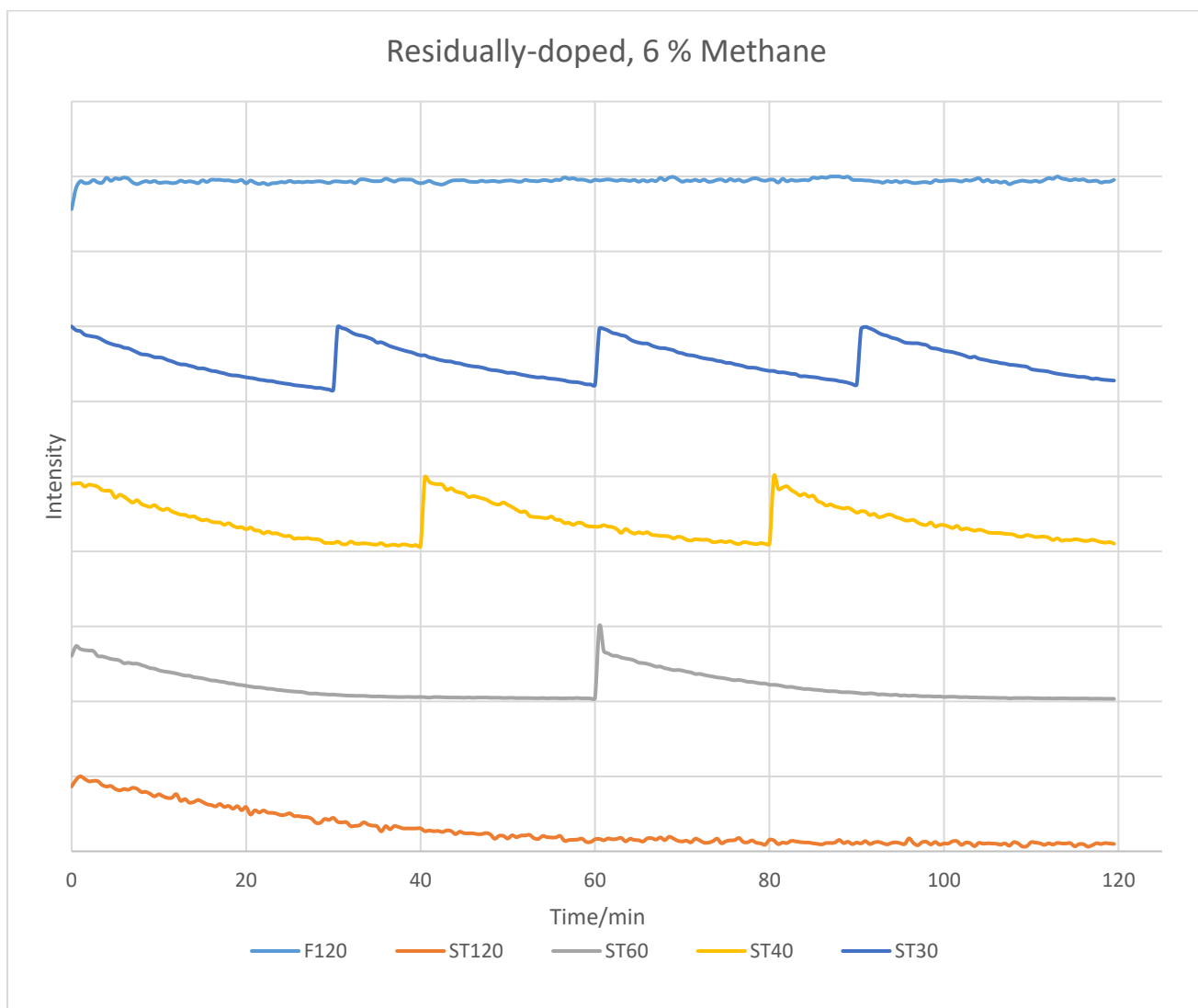


**Figure 26** OES results showing  $C_2$  concentration for the residually-doped 4 % data set.

Very similar results can be observed for the residually-doped 6% data set in **figure 26**. However, a notable difference is the time taken for the  $C_2$  concentration to plateau for this data set. Looking at the ST120 run it takes approximately 50 minutes to plateau whereas in the residual 4 % data set it only took 20 minutes. This is due to the higher concentration of methane. Higher concentration of methane introduced at the start would take longer to be deposited hence the more gradual decrease in methane concentration. With these two data sets OES analysis was simple as the spectra were baseline corrected relative to a peak at 519.3961 nm. This baseline corrected data was then plotted against time and the data was normalised to the highest value of  $C_2$  intensity.

### 6.1.3 4 % Undoped Data

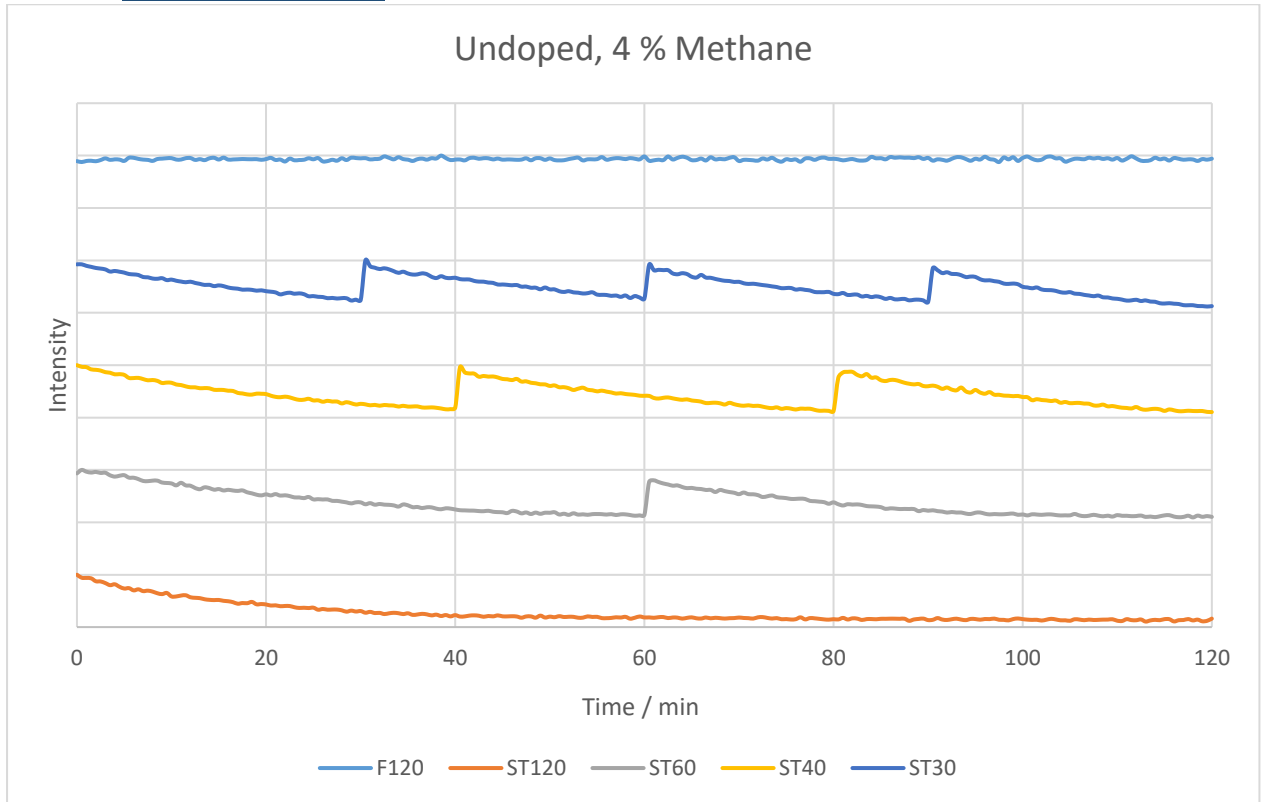


**Figure 27** OES results showing  $C_2$  concentration for the undoped 4 % data set.

The results here show that for our ST30, ST40 and ST60, whenever methane and hydrogen were cycled there was a sharp increase in  $C_2$  concentration. The increases came at the expected times within each run, confirming that cycling of the gases was successful for this data set. The results show similar trends to the residually-doped data sets, however, this had to be analysed differently. These results had to be load level corrected. In the undoped runs, the OES lens was pointed through the top of the chamber looking at the top of the plasma. When the data was analysed in the same way the residually-doped runs had been, the results were very different. This data had been load level corrected. **See appendix for data processing.**

#### 6.1.4 Undoped 6 %

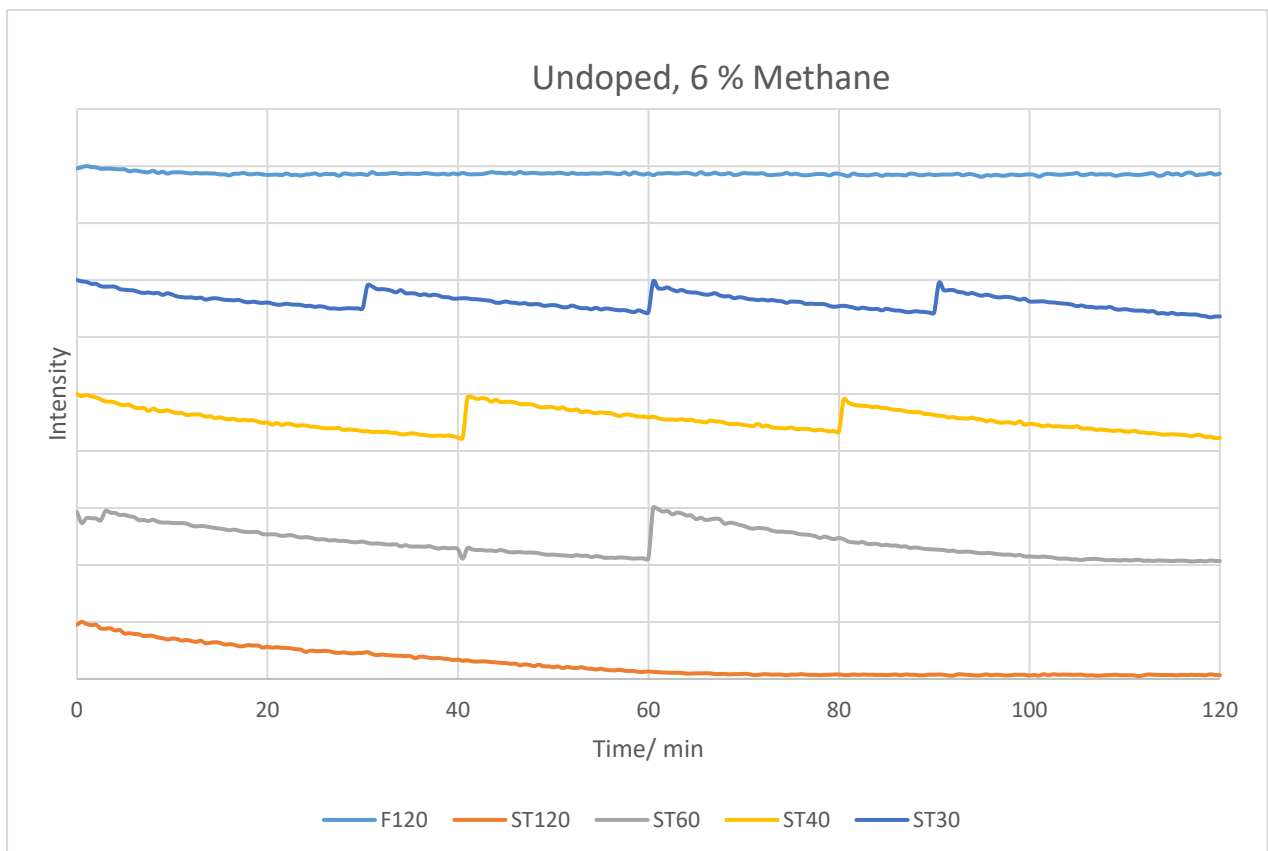


**Figure 28** OES results showing C<sub>2</sub> concentration for the undoped 6 % data set.

The data shown in **figure 28** is consistent with the other data sets. The F120 is approximately constant for the duration of the run. The C<sub>2</sub> curves decay much slower than the undoped 4 % run. This would be due to the increase in methane concentration. For static runs, the gradual decay of the C<sub>2</sub> peak is seen and a sharp increase in intensity when the precursor gases are cycled in, similar to the previous data sets. The baseline for this data set was corrected relative to a peak at 519.4352 nm.

The OES data for this data set was analysed differently to the previous data sets. The C<sub>2</sub> intensity in this set was corrected relative to the hydrogen Balmer-  $\alpha$  peak. **See appendix for data processing.**

For the undoped 4 % and 6 % methane runs the wavelength used to identify the C<sub>2</sub> peak was at 516.4202. Whereas for the residually-doped runs this value was 516.4014. These inconsistencies would be within the standard error on the spectrometers.

### 6.1.5 Time Constants

**Table 6** Showing all the values of the time constants for each run conducted.

	<b>Residually-doped 4 %</b>	<b>Residually-doped 6 %</b>	<b>Undoped 4 %</b>	<b>Undoped 6 %</b>
<b>F120</b>	-	-	-	-
<b>ST120</b>	0.082	0.029	0.038	0.025
<b>ST60</b>	0.087	0.06	0.041	0.044
<b>ST40</b>	0.043	0.049	0.047	0.03
<b>ST30</b>	0.018	0.044	0.063	0.029

For every spectrum, a time constant was calculated. For each run a graph was taken of  $C_2$  against time for 25 minutes of the last decay. The graph was 25 minutes starting from 2 minutes after the precursor gases had been flown in. For example, for the ST30 a graph from 92 minutes to 117 minutes had been plotted. This is because there may be a fluctuation in  $C_2$  intensity when methane is reintroduced. From the OES test shown in **figure 24**, when methane is flowed in initially there is a fairly large spike. Furthermore, the Waves program recorded spectra every 30 seconds. Small changes in the methodology, such as a delay in starting the timer would cause the spectra to take readings at different points, hence provide less reliable results.

It would be expected that each value within a data set would be similar however data shows this was not the case. One reason for this could be because using an exponential decrease equation only factors in the loss of carbon. However, in diamond CVD there is a constant equilibrium where carbon species can always be reintroduced into the gas phase. At the end of a ST30 run and ST120, much more methane has been present during the ST30 run. Therefore, there would be more carbon deposited and more carbon could be desorbed and reintroduced into the gas phase.

There were not many trends shown across the data sets. The ST120, ST40 and ST30 runs from the undoped runs showed higher values for the time constant for the 6 % compared to the 4 %. In the residually-doped 4 % data set the ST120 and ST60 time constant values were much higher than the ST30 and ST40. For the 4 % undoped run the time constant value increased from ST120 to ST30. However, there was not a trend in time constant seen for either of the 6 % methane data sets.

### 6.1.6 Overall

Overall, OES has provided a very useful process monitor for each growth run conducted. This is by providing real-time analysis on the composition of the plasma without disturbing diamond growth. However, it is only an indication of methane concentration and can be affected heavily by problems such as graphite being deposited onto its windows and obstructing the view of the lens.

## 6.2 Raman Spectroscopy

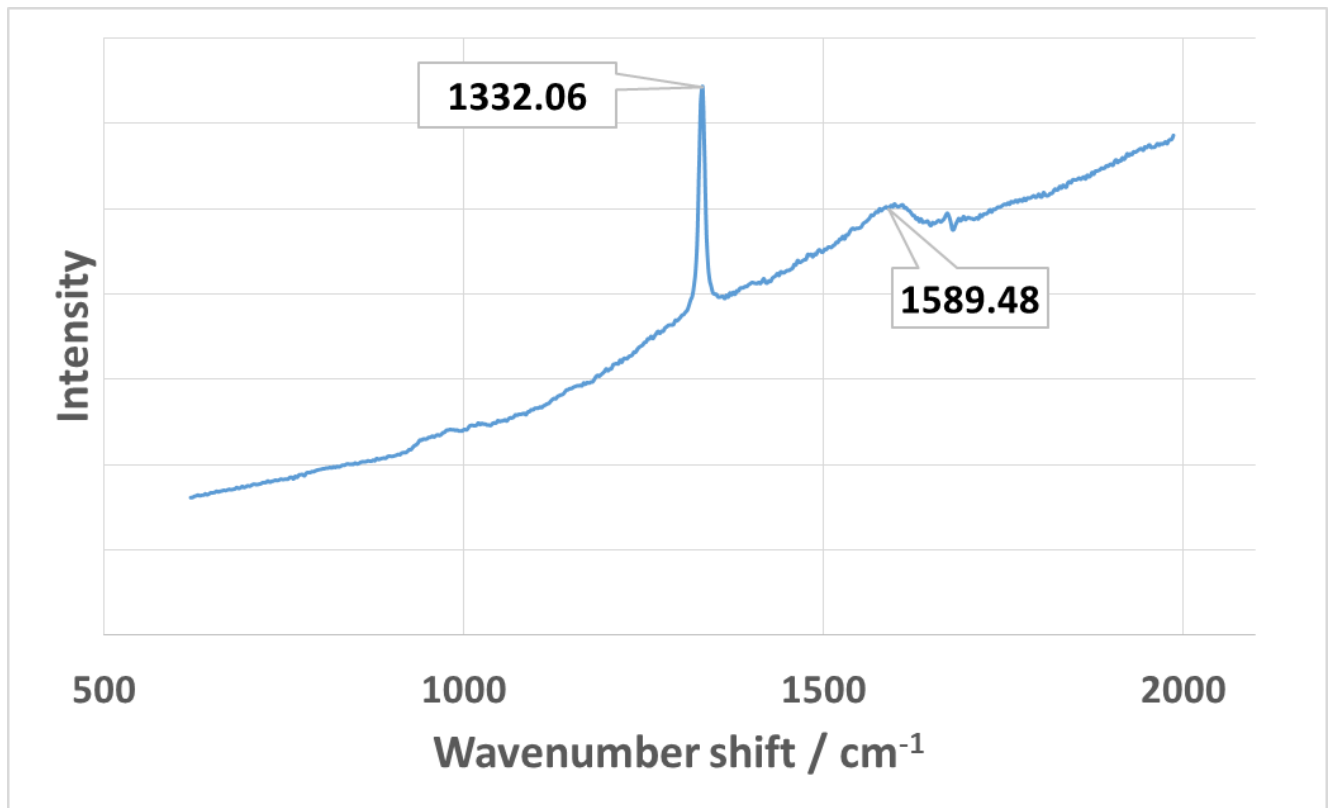


**Figure 29** Raman spectrum taken from the undoped, 4 % methane, and continuous flow run. The diamond peak is highlighted at 1332.06 cm<sup>-1</sup> and the graphite band at 1589.48 cm<sup>-1</sup>.

Raman analysis provides information on the crystallinity and purity of the diamond films grown. The full width half maximum value was recorded for each sample. The smaller this value, the more crystalline the diamond would be. Furthermore, the band present at approximately 1500 cm<sup>-1</sup> shows the presence of graphite impurity within the sample.

### 6.2.1 Undoped 6 % Data Set

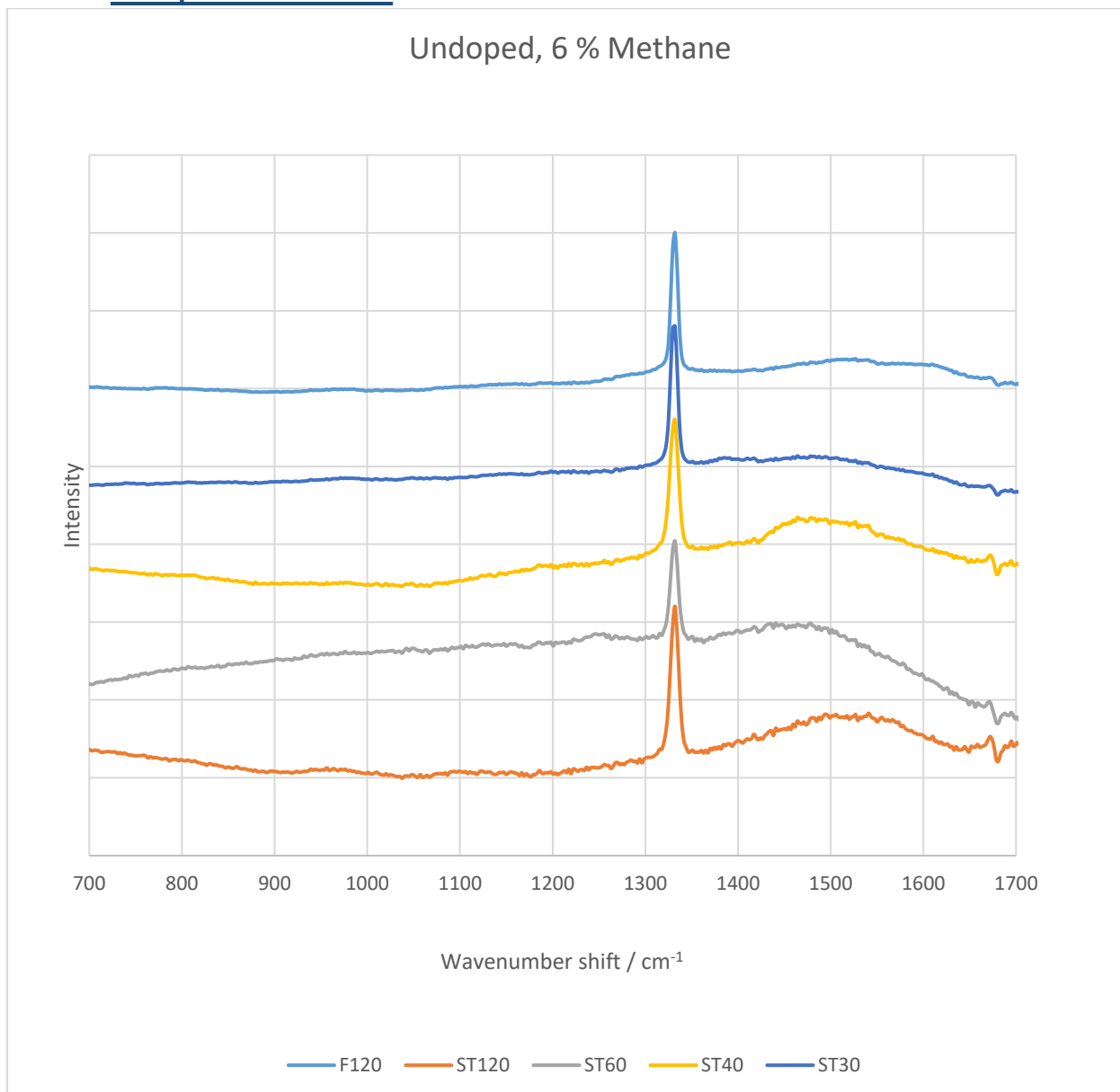


**Figure 30** Raman spectra for the undoped 6 % data set. Data sets have been offset for clarity.

The most crystalline data set was the 6 % methane undoped, this set provided the lowest average full-width half maximum,  $9.301 \text{ cm}^{-1}$ . Within this data, set the most crystalline run was the continuous flow run. Out of the static runs, the ST60 and ST30 provided the most crystalline diamond. However, when inspecting the Raman spectra, this data set was fairly graphitic relative to the other data sets. Hence, the diamond grown here was of low purity. One reason why this data set was graphitic was because of the higher percentage of methane used. With a lower percentage of hydrogen in the chamber, there would be less etching of graphitic residues. The ST120 and ST60 growth runs were the most graphitic. The graphite band was much less prominent for the ST30 growth run. Using the information from this set of conditions alone it can be argued that the ST30 run provides the best diamond as it is of relatively high purity and good crystallinity

## 6.2.2 Undoped 4 % Data Set

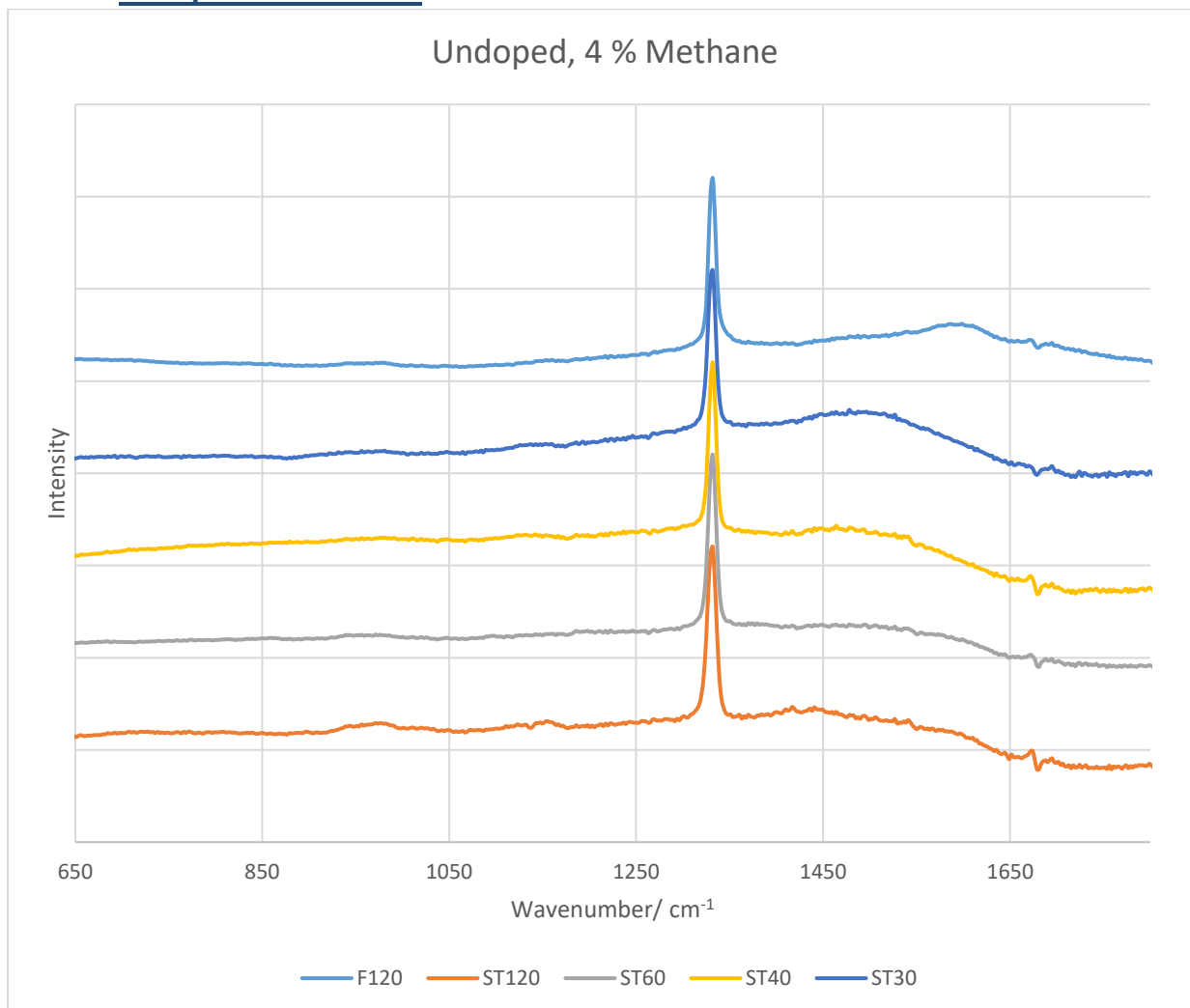


**Figure 31** Raman spectra for the undoped 4 % data set. Data sets have been offset for clarity.

The second most crystalline data set was the 4 % methane undoped, with the second smallest average full width half maximum,  $9.703 \text{ cm}^{-1}$ . Within this data set the ST60 and ST40 growth runs had the best crystallinity and the ST120 was the most crystalline, this was also seen in the 6 % methane undoped data set. Overall, this set was much less graphitic than the 6 % methane undoped. This is expected as a lower concentration of methane was used. With a higher percentage of hydrogen present the graphitic residues were etched away more efficiently. However, the ST30 run in this data set was the most graphitic relative to the rest of the data set. By inspection, the ST60 seemed to be the least graphitic within this data set.

### 6.2.3 Residually-doped 4 %

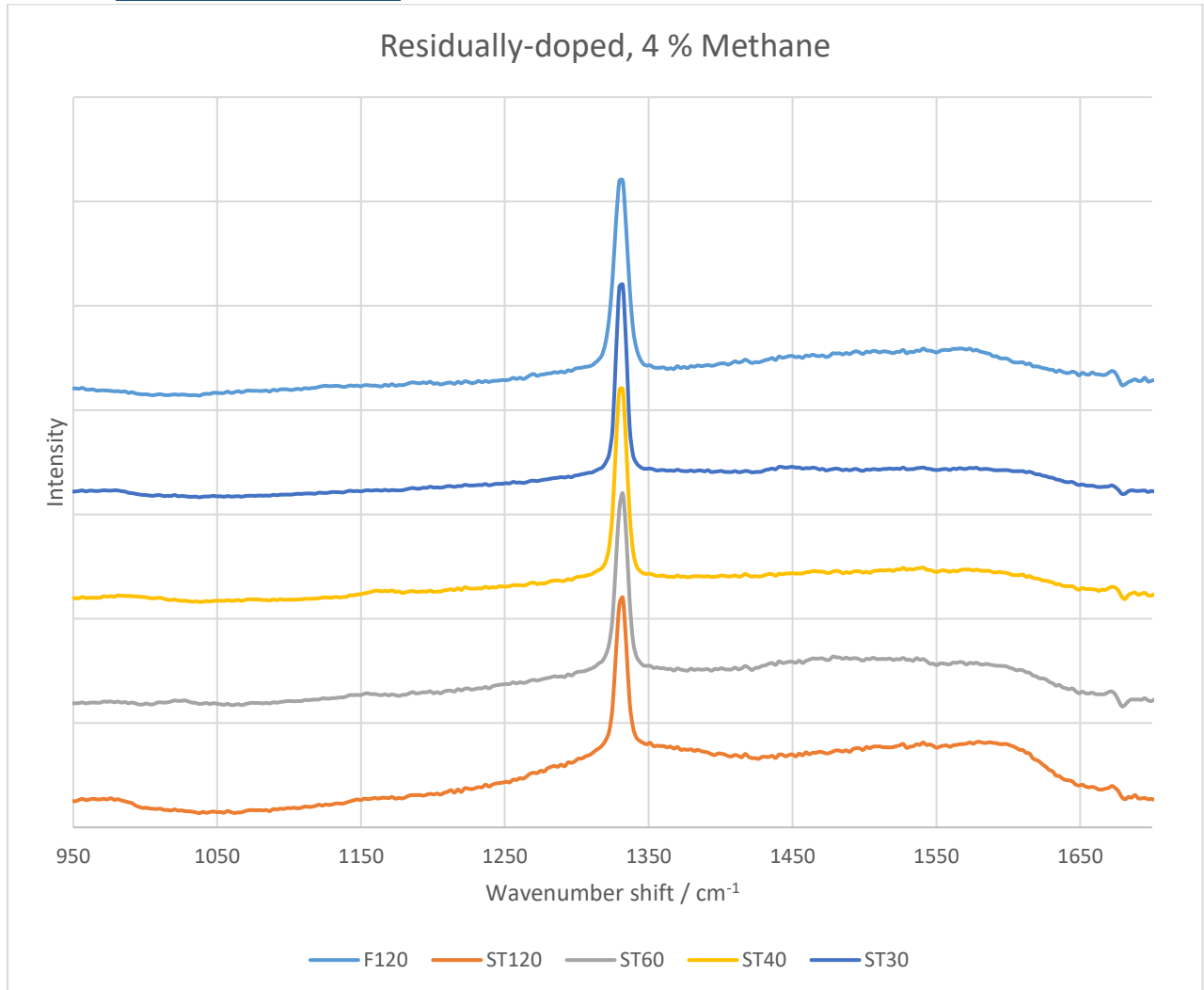


**Figure 32** Raman spectra for the residually-doped 4 % data set. Data sets have been offset for clarity.

The residually-doped 4 % data set was the third most crystalline data set. With a full width half maximum average of 9.767 cm<sup>-1</sup>. Within this data, set the ST40 and ST60 provided the most crystalline diamond. The least crystalline growths within this set were the ST120 and ST30 static growth runs. The growth runs from this set were generally the least graphitic relative to the other data sets, hence provided the highest purity of diamond. Within this set, the ST40 and ST30 growths provided relatively pure diamonds, whereas the ST120 provided the least pure. However, this data set as a whole had relatively low amounts of graphite present on the films.

## 6.2.4 Residually-doped 6 %

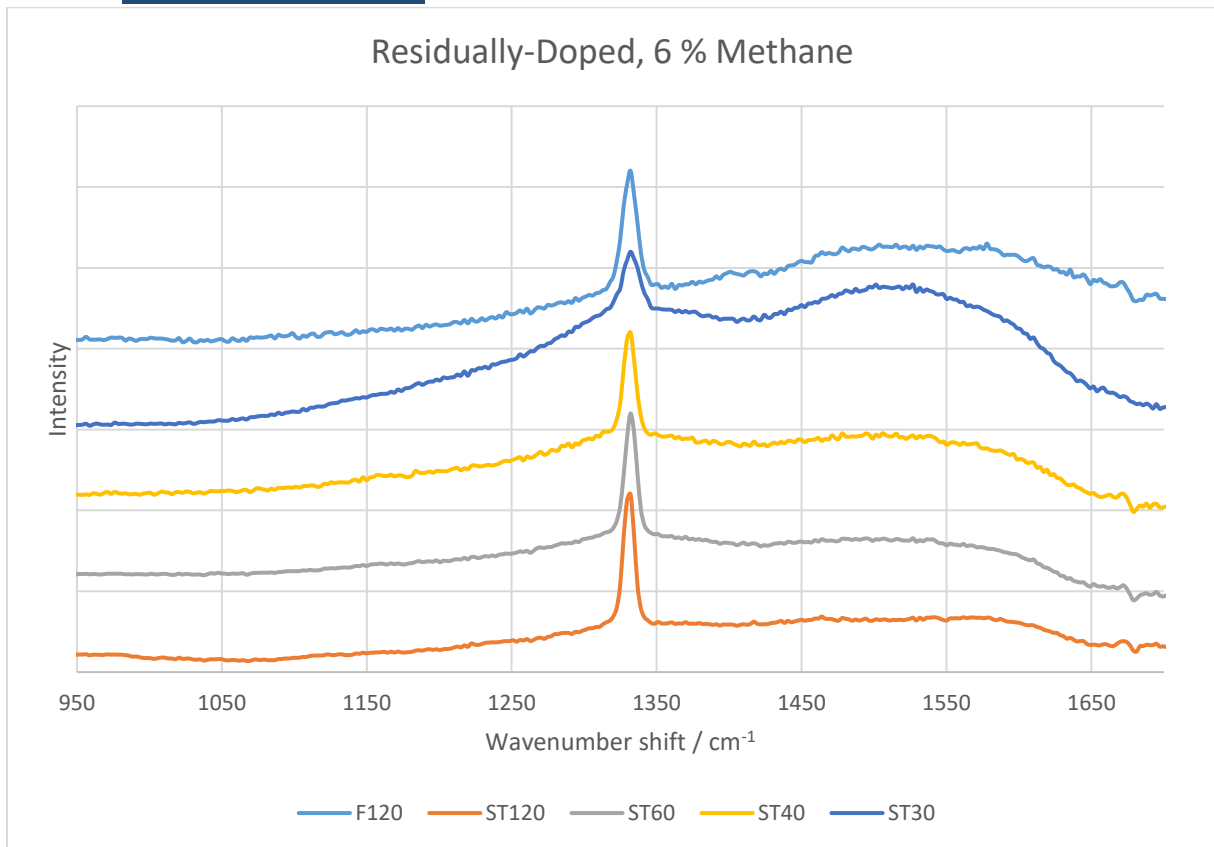


**Figure 33** Raman spectra for the residually-doped 6 % data set. Data sets have been offset for clarity.

The data set which provided the least crystalline diamonds was the 6 % residually-doped data set. The average full width half maximum for this data set was 10.302 cm<sup>-1</sup>. This was excluding the ST40 data because the curve fitting was inadequate. The ST60 and ST120 showed the most crystalline diamond growths within this data set whereas the ST30 growth run was the least crystalline out of the static flow runs. The substrate used for the ST40 growth was off centre and provided a gradient across the sample. One side of the substrate was highly graphitic whilst the other side had some diamond growth present. This data set seemed much more graphitic than the residually-doped 4 % data set and less graphitic than the undoped 6 % data set. However, the ST30 growth in the residually-doped 6 % data set was much more graphitic compared to the ST30 in the undoped 6 % data set.

### 6.2.5 Overall

Generally, the undoped data sets provided more crystalline diamond films compared to the residually-doped data sets with the undoped 6 % being the most crystalline set. This is expected because the presence of a dopant that could manifest itself within a lattice would disrupt its crystallinity. However, the diamond from the residually-doped data sets were much purer, showing the least amount of graphite. The purest data set being the 4 % residually-doped. This data is consistent with literature where studies have shown that the presence of boron dopant can help reduce graphitic components.<sup>66</sup>

Within both undoped data sets, the ST30 and ST60 provided consistently high crystalline diamond. The 6 % undoped ST30 provided fairly high purity diamond so this may be the best option. In the residually-doped data sets, the 6 % set has the lowest crystallinity and lower purity than the 4 % residual data set. Within the 4 % set the ST40 and ST60 runs were the most crystalline. Therefore, high purity and high crystallinity diamond can be grown using both systems, however the static run cycles and methane concentration must be correctly chosen for the system used. In general, the ST60 cycles provided good crystallinity across each of the data sets.

### 6.3 Scanning Electron Microscopy

Scanning electron microscopy (SEM) was used to provide cross sectional images of the diamond films. From this thickness was measured and growth rates were calculated. Images were taken near the edge and in the centre of the film, giving some indication on uniformity.

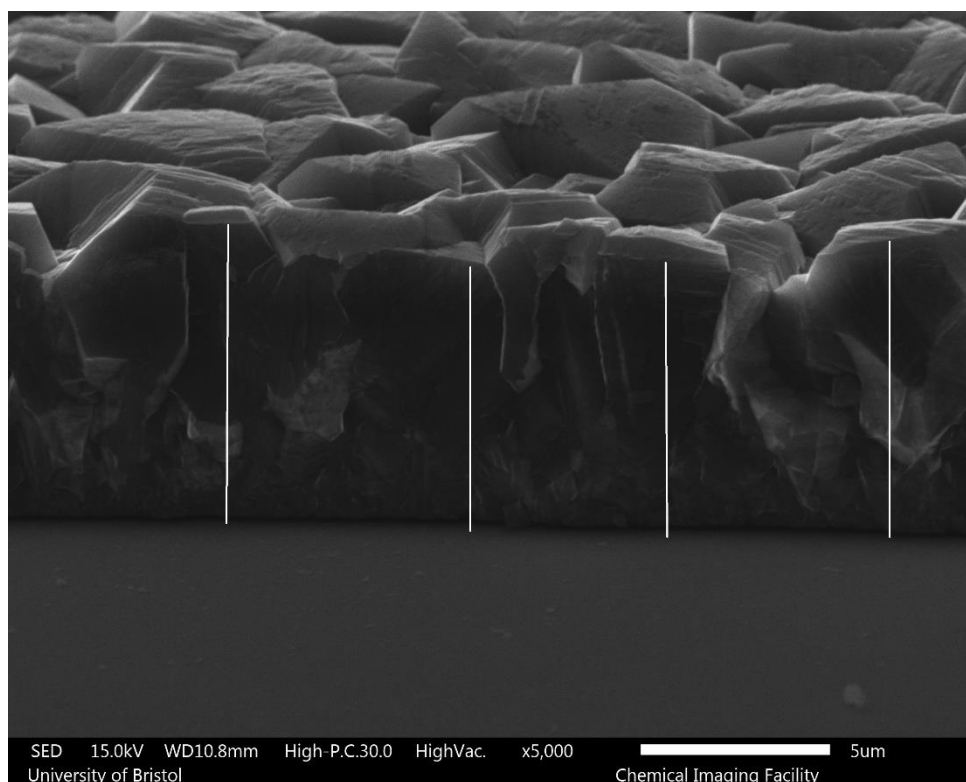


**Figure 34** SEM image taken from the edge of the ST30, 6 %, undoped run. Lines are drawn across the sample. Using the pixel counter on paint these lines could be measured in pixels and converted to  $\mu\text{m}$  using the scale bar and measuring the scale bar in pixels. An average of the 4 lines was taken for analysis.

### 6.3.1 6 % Residually-Doped

Table 7 showing the thicknesses and growth rates for the residually-doped 6 % data set.

<u>6%, Residually-Doped</u>	<u>Thickness Middle/ <math>\mu\text{m}</math></u>	<u>Thickness Edge/ <math>\mu\text{m}</math></u>	<u>Growth Rate Middle/ <math>\mu\text{m h}^{-1}</math></u>	<u>Growth Rate Edge/ <math>\mu\text{m h}^{-1}</math></u>
F120	14.91	15.98	7.45	7.99
ST30	13.84	13.84	6.92	6.92
ST40	13.84	10.65	6.92	5.32
ST60	10.64	9.58	5.32	4.79
ST120	2.93	2.13	1.20	1.06

Generally, this data set showed the quickest growth rates, with the continuous flow run showing the highest growth rate of  $7.45 \mu\text{m h}^{-1}$ . Out of the static flow runs, ST30 and ST40 provided the highest growth rates. This would be because, for these runs, methane was added relatively frequently. By adding more methane during the run, more deposition would be expected as there is a higher amount of carbon. This is supported by the results of the ST120 run, which provided the lowest growth rate from this data set, as methane was only added at the beginning of the run. Comparing the growth rates from the edge and the middle of the sample, ST30 is the most uniform diamond film from this set, whereas the ST40 is the least uniform. ST40 has a difference of  $3.19 \mu\text{m}$  between the edge and the centre of the film. The reason for this big difference would most likely be due to the substrate being off centre. During the ST40 run, it was visible that the substrate was off centre and wasn't completely engulfed by the ball of the plasma leading to uneven deposition. When working under these conditions, ST30 would be ideal in providing high growth rates and a uniform diamond film.

### 6.3.2 6 % Undoped

**Table 8** showing the thicknesses and growth rates for the undoped 6 % data set.

<u>6%, Undoped</u>	<u>Thickness Middle/ <math>\mu\text{m}</math></u>	<u>Thickness Edge/ <math>\mu\text{m}</math></u>	<u>Growth Rate Middle/ <math>\mu\text{mh}^{-1}</math></u>	<u>Growth Rate Edge/ <math>\mu\text{mh}^{-1}</math></u>
F120	4.79	4.25	2.40	2.26
ST30	10.12	8.52	5.06	4.26
ST40	10.12	9.58	5.06	4.79
ST60	9.59	7.99	4.79	3.99
ST120	6.92	6.92	3.46	3.46

The undoped 6 % methane data set provided generally lower growth rate values than the residually-doped 6 %. One major point here is that the F120 run gave the lowest growth rate whereas in the 6 % residually-doped data set it was the highest. The reason for this is unclear. One possible explanation could be the leak rate of the different chambers used. A leak rate would have a major impact on static flow growth. The presence of nitrogen and oxygen can increase the growth rate of diamond films. This is because, with static flow, gases aren't being constantly pumped out, so nitrogen that enters the chamber will remain. However, for continuous flow runs the gases are constantly being pumped out, including any impurities. If one chamber has a much higher leak rate than the other, this could greatly increase the static flow growth runs relative to the continuous flow growth runs.

Out of the static runs for this data set, the ST30 and ST40 provided the highest growth rates whilst the ST120 provided the lowest. This is similar to the trend observed in the residually-doped 6 % data set. In general, this data set showed much less uniformity in the diamond films compared to the 6 % residually-doped set. However, ST30 is much less uniform with a difference of 1.6  $\mu\text{m}$  between the edge and centre of the sample. The ST120 and F120 showed relatively high uniformity within this set. Under these conditions, ST40 seems like the best static flow option providing a high growth rate, but better uniformity than the ST30 diamond. Another noticeable difference between the two 6 % data sets is that the undoped ST120 had a much higher growth rate than the residually-doped. One possible explanation for this could, again, be due to leak rate, if the undoped chamber had a higher leak rate, this would lead to a higher growth rate for one chamber compared to the other.

### 6.3.3 4 % Undoped

**Table 9** showing the thicknesses and growth rates for the undoped 6 % data set.

<u>4%, Undoped</u>	<u>Thickness Middle/ µm</u>	<u>Thickness Edge/ µm</u>	<u>Growth Rate Middle/ µmh<sup>-1</sup></u>	<u>Growth Rate Edge/ µmh<sup>-1</sup></u>
F120	5.32	3.35	2.66	1.68
ST30	7.99	7.99	3.99	3.99
ST40	7.61	7.72	3.80	3.86
ST60	6.39	5.85	3.19	2.92
ST120	5.32	5.32	2.66	2.66

Similar to the 6 % undoped data set, the F120 and ST120 runs had the poorest growth rate. The ST30 and ST40 runs provided the highest growth rates for this set. For all static runs relatively high uniformity is seen, the ST30 and ST120 providing the most uniform diamond films. However, the continuous flow run had poor uniformity, showing a difference in thickness of 1.97 µm between the centre and the edge. Although the trends in this set were similar to the undoped 6 % data set, each growth rate was much lower. This is expected as a lower concentration of methane was used. Lower percentages of methane present would mean less carbon that could be deposited, hence a thinner diamond film.

### 6.3.4 4 % Residually-Doped

Table 10 showing the thicknesses and growth rates for the undoped 6 % data set.

<u>4%, Residually-Doped</u>	<u>Thickness Middle/ µm</u>	<u>Thickness Edge/µm</u>	<u>Growth Rate Middle/ µmh<sup>-1</sup></u>	<u>Growth Rate Edge/ µmh<sup>-1</sup></u>
F120	8.51	8.52	4.26	4.26
ST30	4.25	4.26	2.13	1.86
ST40	4.25	4.26	2.13	1.86
ST60	3.72	3.73	1.86	1.60
ST120	1.05	1.06	0.53	0.53

Generally, the residually-doped 4 % data set provided the overall lowest growth rates. Similar to the other data sets the ST30 and the ST40 provided the highest growth rates and the ST120 provided the lowest. Furthermore, similar to the residually-doped 6 %, the flow run here was the highest growth rate within the data set. This is further evidence to suggest that there is a significant difference in air leak rate between the two chambers. This is because, for both residually-doped sets the flow runs had the highest growth rate whereas for the undoped sets they had the lowest. This suggests a difference in the reactor chambers used for these experiments, such as an air leak. Within this data set, the ST30 and ST40 runs provided the most uniform diamonds, whereas the ST30 and ST40 provided the least uniform. Both of them having a difference in thickness of 0.53 µm.

### 6.3.5 Overall

Overall, the ST30 and ST40 runs consistently outputted the highest growth rates across all the data sets compared to the other static cycles. This would be due to methane being flowed into the chamber much more regularly than the ST60 and ST120 growth runs. The residually-doped 6 % set provided the highest growth rates and the 4 % methane outputted the lowest growth rates. Furthermore, using 6 % methane compared to 4 % shows an overall increase in growth rate for the static cycles. This is because the more methane is being flowed into the chamber each time the precursor gases are cycled in. There was little trend in uniformity across the sets. However, the ST30 runs within the 6 % residually-doped

and 4 % undoped data sets showed high uniformity and relatively high growth rates. The ST120 and F120 runs had relatively good uniformity across each data set. However, the ST120 consistently outputted poor growth rates and the F120 outputted poor growth rates for the undoped data sets.

## 7 Conclusions

### Summary

The aim of this research was to investigate static flow cycles. Methane concentration, static cycles and chamber conditions were varied. Results have shown that no one cycle would provide the best solution. The parameters: carbon economy, growth rate, purity and crystallinity cannot all be optimised using a single method. In order to improve one parameter, at least one other parameter will be worsened.

From Raman data, it was shown that using an undoped chamber would generally provide a better crystallinity. Whereas, for the residually-doped chamber, higher purities were observed. Depending on which chamber condition is chosen, static cycle must be chosen. For example, in the 6 % undoped data set, the ST30 was less crystalline than the ST60, but had a higher purity. However, this trend is not applicable across all data sets as the opposite was seen in the residually-doped 6 % data set, where the ST120 run was more crystalline and had higher purity than the ST30. A general trend in chamber conditions was that the undoped chamber provided higher crystallinity, whereas the residually-doped chamber provided less graphitic diamond.

Trends from the SEM data showed that 6 % methane concentration generally provided higher growth rates. The residually-doped 6 % data set was shown to have a higher growth rate than the 6 % undoped set, however the opposite was seen for the two 4 % data sets. It was seen that generally ST30 and ST40 cycles provided higher growth rates out of the static runs. However, these static cycles require the use of more methane, which may be counterproductive if you want to minimise the amount of methane used. Therefore, a balance between carbon economy and growth rate must be made.

Furthermore, it was seen that using a higher percentage of methane would provide a lower purity and worse carbon economy, even though higher growth rates were outputted.

It has been demonstrated that good quality diamond can be grown using static flow cycles. The method for diamond growth using a static flow cycle should be chosen based on what parameters are prioritised. For example, if growth rate was prioritised, then flowing methane in every 30 minutes should be the chosen cycle.

This research is beneficial to the construction of a diamond battery because it investigates the effects of carbon economy on purity, crystallinity and growth rate of diamond. For a diamond battery carbon-14 would be used which is highly radioactive and very expensive. Therefore, the carbon economy parameter should be optimised so that low amounts of carbon-14 methane may be used. Depending on which other parameters are prioritised, a suitable method can be chosen. High crystallinity can improve the electronic properties of diamond such as, electron mobility. Therefore, this would be another parameter that should be prioritised. One method that provides highly crystalline diamond using low carbon economy was the ST60 run, with residually-doped chamber conditions and using 4 % methane. This growth provided relatively high crystallinity and used a lower percentage of methane, with the methane being flowed in twice.

## **Future Work**

OES in the future could be very useful for being conservative with the precursor gases whilst also providing a high quality diamond deposition. Once the C<sub>2</sub> intensity drops below a certain level, a system could be in place to automatically cycle in the precursor gases for a designated amount of time. Research should proceed into discovering at what C<sub>2</sub> intensity the diamond quality begins to degrade. When the optical emission spectrum shows C<sub>2</sub> reaching this intensity, the precursor gases could be cycled in. This would lead to maximum efficiency with the precursor gases whilst not degrading the quality of diamond.

Furthermore, the differences in flow runs between the residually-doped and undoped chamber conditions should be researched. For the residually-doped data set the flow runs provided the highest growth rate whereas they provided the lowest growth rate for the undoped data set. As a starting point, leak rate tests should be conducted on each chamber to determine whether an air leak is the cause for this difference.

Additionally, the residually-doped chamber could be fully pumped down until a negligible diborane concentration remained. Several 'undoped' growth runs can then be conducted in this chamber, followed by residually-doped runs. The significance of this is that a direct comparison can be drawn between these two chamber conditions. Environment of the chamber, for example, whether one has gas lines in a warmer environment, could change the gas flows. Other differences include MFCs, gas line configuration and source of gases. Two different reactors were used for the undoped and residually-doped runs, where the parameters mentioned were different for each reactor. Doing tests on the exact same reactor could provide more clarity on how residually-doped and undoped conditions impact diamond growth.

Further research can be done to be as economical as possible with methane, whilst providing high purity and highly crystalline diamond. Parameters such as these being optimised, would provide aid to the construction of a diamond battery.

## 8 References

1. P. Hartmann, R. Haubner and B. Lux, *Diamond and Related Materials*, 1996, **5** 850-856
2. J. C. Angus, *Diamond and Related Materials*, 2014, **49**, 77-86.
3. M. C. S. Africa, Uses of diamond, <https://www.miningforschools.co.za/lets-explore/diamond/uses-of-diamonds>, (accessed 12/21/21, 2021).
4. J. E. Graebner, *Diamonds: Electronic Properties and Applications*, 1995.
5. C. A. M. E.J.D, H. Dominguez-Andrade, A. M.N.R and N. A. Fox, *Diamond and Related Materials*, 2020, **109**.
6. C. J. H. Wort and R. S. Balmer, *Materialstoday*, 2008, **11**, 22-28.
7. E. H. Wahl, PhD, Stanford University, 2002.
8. D. Qi, Diamonds Could Be The 'Crown Jewel' In Future Electronics<path clip-rule="evenodd" d="M28.5 1.2A27.45 27.45 0 0 4.06 15.82L3 15.27A28.65 28.65 0 0 1 28.5 0C39.64 0 49.29 6.2 54 15.27l-1.06.55A27.45 27.45 0 0 28.5 1.2zM4.06 41.18A27.45 27.45 0 0 28.5 55.8a27.45 27.45 0 0 24.44-14.62l1.06.55A28.65 28.65 0 0 1 28.5 57 28.65 28.65 0 0 1 3 41.73l1.06-.55z" fill-rule="evenodd">, <https://medium.com/thelabs/diamonds-could-be-the-crown-jewel-in-future-electronics-40b1211e91a1>, (accessed 13/01/2022).
9. S. Sattel, How Schottky Diodes Work, <https://www.autodesk.com/products/eagle/blog/schottky-diodes/>, (accessed 14/01/2022).
10. European-MRS, Diamond for electronic devices, <https://www.european-mrs.com/diamond-electronic-devices-emrs>, (accessed 14/01/2022).
11. R. I. Database, RefractiveIndex.info, <https://refractiveindex.info/?shelf=3d&book=crystals&page=diamond>, (accessed 22/12/21).
12. H. De Wit, Understanding Diamond and its Relationship with Optics, <https://www.photoniconline.com/doc/understanding-diamond-and-its-relationship-with-optics-0001>, (accessed 22/12/2021).
13. L. Blain, Arkenlight to commercialize nuclear diamond betavoltaic batteries, <https://newatlas.com/energy/arkenlight-nuclear-diamond-batteries/>, (accessed 21/03/2022).
14. E. Fermi, *The Physics of Diamond*, IOS Press, Amsterdam, Netherlands, 1997.
15. M. Rossi, How Can Diamond and Graphite be So Different if they're Both Composed of Pure Carbon, <https://www.scientificamerican.com/article/how-can-graphite-and-diam/>, (accessed 22/21/2021).
16. M. E. Thomas and W. J. Tropf, *SPIE*, 1994, **2286**, 16-23.
17. M. Chandran, *Carbon-Based Nanofillers and Their Rubber Nanocomposites*, Amsterdam Elsevier, Amsterdam, 2019.
18. P. W. May, *Philosophical Transactions of the Royal Society*, 2000, **358**, 473-495.
19. D. V. Feedosev, K. S. Uspenskaya, V. P. Varnin and S. P. Vnukov, *Izv Akad Nauk SSSR, Seriya Khim.*, 1978, **6**, 1252-1256.
20. D. N. Belton and S. J. Schmeig, *Surf.Sci*, 1990, **233**, 131-140.
21. P. W. May, J. N. Harvey, N. L. Allan, J. C. Richley and Y. A. Mankelevich, 2010, *Journal of Applied Physics*, **108**, 014905
22. K. Benzhoura, J. Szatkowskib, F. Rozplochb and K. Stecb, *Acta Physics Polonica, Series A (Online)*, 2010, **118**, 447-449.
23. D. C. Barbosa, M. R. Baldan, V. Trava-Airoldi, E. J. Corat and U. A. Mengui, *Material Science Forum*, 2016, **869**, 721-726.

24. J. J. Gracio, Q. H. Fan and J. C. Madaleno, *Journal of Physics D: Applied Physics*, 2010, **43**, 1-57.
25. R. S. o. Chemistry, Tungsten- Elemental information, <https://www.rsc.org/periodic-table/element/74/tungsten>, (accessed 26/12/2021).
26. R. S. o. Chemistry, Tantalum- Elemental Information, <https://www.rsc.org/periodic-table/element/73/tantalum>, (accessed 26/12/2021).
27. W. Ahmed, S. M. Jackson, C. Rego, I. U. Hassan, K. Subramani and J. Yazdani, *Emerging Nanotechnologies in Dentistry*, Elsevier Science Publishing Co Inc, 2012.
28. G.-R. Lai, E. N. Farabaugh, A. Feldman and L. H. Robins, *Journal of Research of the National Institute of Standards and Technology*, 1995, **100**, 43-49.
29. M. N. R. Ashfold, Lecture Series: Probing The Gas Phase Chemistry Involved in Chemical Vapour Deposition (CVD), <https://slideplayer.com/slide/782375/>, (accessed 29/03/2022).
30. T. D. Moustakas, *Solid State Ionics*, 1989, **32-33**, 861-868.
31. K. Kobashi, *Diamond Films*, Elsevier Science, 2005.
32. M. Roy, *Materials Under Extreme Conditions*, Elsevier Science, 2017.
33. S. M. Leeds, Doctor of Philosophy, University of Bristol, 1999.
34. K. Kurihara, K. Sasaki and M. Kawarada, *MATERIAL AND MANUFACTURING PROCESSES*, 1991, **6**, 241-256.
35. J. Laimer, C. Pauser, G. Schwarzler and H. Stori, *Surface Coatings and Technology*, 1998, **98**, 1066-1071.
36. T. B. Huang, W. Z. Tang, F. X. Lu, N. Ali and J. Gracio, *Thin Solid Films*, 2003, **429**, 108-113.
37. F. X. Lu, W. Z. Tang, T. B. Huang, J. M. Liu, J. H. Song, Y. Yu and M. Tong, *Diamond and Related Materials*, 2001, **10**, 1551-1558.
38. M. A. Al Mamun, H. Furuta and A. Hatta, *Materialstoday Communications*, 2018, **14**, 40-46.
39. W. S. Lee, K. W. Chae, K. Y. Eun and Y. J. Baik, *Diamonds and Related Materials*, 2001, **10**, 2220-2224.
40. E. Britannica, Carbon-14 dating, <https://www.britannica.com/science/carbon-14-dating>, (accessed 06/01/2022).
41. M. Noda, *J. Indian Inst. Sci*, 2001, **81**, 627-636.
42. S. Sciortino, S. Lagomarsino, F. Pieralli, E. Borchini and E. Galvanetto, *Diamond and Related Materials*, 2002, **11**, 573-578.
43. D. K. Rai, D. Datta, S. K. Ram, S. Sarkar, R. Gupta and S. Kumar, *Solid State Sciences*, 2010, **12**.
44. D. Lundin and H. Pederson, *Physics Procedia*, 2013, **46**, 3-11.
45. B. A. K. Reshi, S. Misra, A. Varma, R. *Material Research Express*, 2019, **6**, 046407.
46. M. R. Derakhshandeh, M. J. Eshraghi, M. M. Hadavi, M. Javaheri, S. Khamseh, M. G. Sari, P. Zarrintaj, M. R. Saeb and M. Mozafari, *Surface Innovations*, 2018, **6**, 167-175.
47. S. Shikata, *Diamond and Related Materials*, 2016, **65**, 168-175.
48. J.-C. Arnault, S. Saada and V. Ralchenko, *Physics Status Solidi RRL*, 2021, **2100354**.
49. M. Schreck, J. Asmussen, Shikata S, J.-C. Arnault and N. Fujimori, *MRS Bulletin*, 2014, **39**, 504-510.
50. R. Linares and P. Doering, *Diamond and Related Materials*, 1999, **8**, 909-915.
51. M. J. Verstraetea and J.-C. Charlier, *Applied Physics Letters*, 2005, **86**, 191917.
52. S. Gsell, T. Bauer, J. Goldfu ù, M. Schreck and B. Stritzker, *Applied Physics Letters*, 2004, **84**, 4541-4543.
53. E. J. D. Mahoney and B. S. A. Truscott, M N R Mankelevich, Yu A, *The Journal of Physical Chemistry A*, 2017, **121**, 2760-2772.
54. J. Ma, M. N. R. Ashfold and Y. A. Mankeevich, *Journal of Applied Physics*, 2009, **105**, 043302.
55. S. Bulou, L. Le Brizoual, R. Hugon, L. De Poucques, M. Belmahi, H.-N. I. Migeon and J. Bougdira, *Plasma Processes and Poylmers*, 2009, **6**, 576-581.

56. A. Chingsungnoen, J. I. B. Wilson, V. Amornkitbamrung, C. Thomas and T. Burinprakhon, *Plasma Sources Science and Technology*, 2007, **16**, 434-440.
57. E. Instruments, What is Raman Spectroscopy?, <https://www.edinst.com/blog/what-is-raman-spectroscopy/>, (accessed 09/01/2022).
58. J. Filik, *spectroscopyeurope*, 2005, **17**, 10-17.
59. S. Praver and R. J. Nemanich, *Philosophical Transactions of the Royal Society A*, 2004, **362**, 2537–2565.
60. A. Dychalska, P. Popielarski, W. Frankow, K. Fabisiak, K. Paprock and M. Szybowicz, *Materials Science-Poland*, 2015, **33**, 799-805.
61. N. Raval, R. Maheshwari, D. Kalyane, S. R. Youngren-Ortiz, M. B. Chougule and R. K. Tekade, *Basic Fundamentals of Drug Delivery*, Elsevier Science, 2019.
62. P. University, Scanning Electron Microscope, <https://www.purdue.edu/epps/rem/laboratory/equipment%20safety/Research%20Equipment/sem.html>, (accessed 31/01/22).
63. M. Omid, A. Fatehinya, Z. Akbarr, S. Shahmoradi, F. Yazdian, M. R. Tahiri, K. Moharamzadeh, L. Tayebi and D. Vashae, *Biomaterials for Oral and Dental Tissue Engineering*, Woodhead Publishing, 2017.
64. A. A. Zolotukhin, R. R. Ismagilov, M. A. Dolganov and A. N. Obraztsov, *Journal of Nanoelectronics and Optoelectronics*, 2012, **7**, 22-28.
65. O. P. Choudhary and P. Choudhary, *International Journal of Current Microbiology and Applied Sciences*, 2017, **6**, 1877-1882.
66. X. H. Wang, G.-H. M. Ma, Z. W, J. T. Glass, L. Bergman, K. F. Turner and R. J. Nemanich, *Diamond and Related Materials*, 1992, **1**, 828-835.

## **9 Appendix**

### **9.1 Section A - PDR**

Some test growth runs were conducted on the PDR. Three runs were done on the PDR. A 2 hour static flow run. A 2 hour continuous flow run that was cut short because the pump had stopped working. Following this a 1 hour continuous flow run had been conducted. The pulse frequency on the PDR is 125 kHz. The MFCs and all the gas valves were controlled using a Delphi computer program. This relayed information to a raspberry pi which then relayed information to the reactor.

#### **Continuous flow start up:**

The chamber was pumped down to approximately 10 mTorr. Hydrogen was flowed in at a rate of 500 sccm and the pressure was set to 2 Torr. Once this pressure was reached, the pinnacle plus power supply was turned on and a plasma struck at 70 W. The pressure dial was set to 180 Torr and power dialled up with an approximate ratio of 10:1 power to pressure. When 100 T is reached, methane was flowed in at 25 sccm. When 100 Torr is reached the power was dialled up quicker until 3 kW is reached when pressure reached 180 Torr.

#### **Static flow start up:**

The chamber was pumped down to approximately 10 mTorr. Hydrogen was flowed in at a rate of 500 sccm and the pressure was set to 2 Torr. The plasma was struck at 70 W. The pressure dial was set to 100 T and power was slowly increased with an approximate 10:1 power to pressure ratio. When 100 T is reached methane was flowed in for 2 minutes at 25 sccm. The pressure dial was then set to 180 Torr and power was increased until 3 kW is reached. At this point, gas flows and vacuum pump were closed.

#### **Shut Down:**

The power was dialled slowly to 0 and the power the supply was turned off. Hydrogen was flowed for 2 minutes. The chamber was pumped down fully after the gas flows off were closed. When the chamber reached approximately 10 mTorr argon was flowed into the chamber. When atmospheric pressure is reached, the chamber was carefully opened to air and sample retrieved.

## PDR Raman

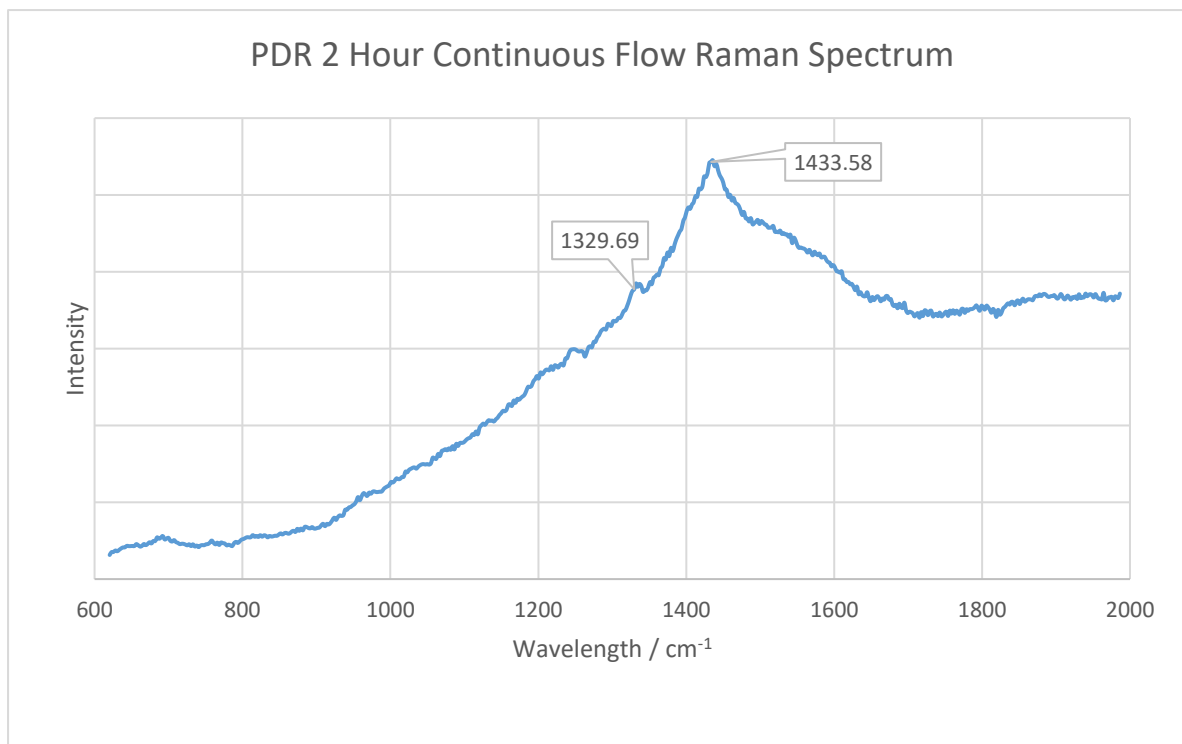


**Figure 35** Raman spectrum from the 2 hour continuous flow run conducted on the PDR that was stopped after 1 hour.

From the Raman spectrum in **figure 35**, a very small peak is seen at 1329.69, this indicates that some  $sp^3$  carbon has been deposited. However, much graphite has been deposited, indicated by the broad band at approximately 1433  $cm^{-1}$ . Overall, this was an unsuccessful diamond growth as the diamond peak is much smaller than the graphite peak.

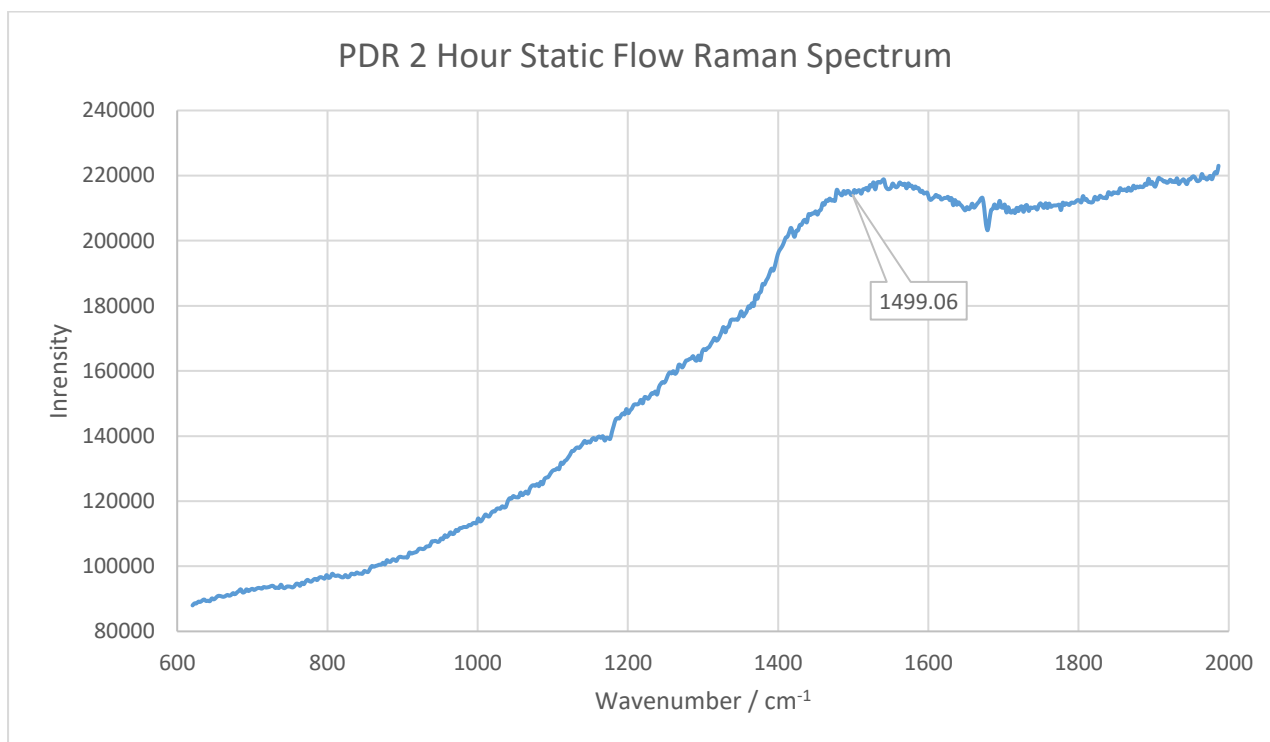


**Figure 36** Raman spectrum from the 2 hour static flow run on the PDR.

The Raman spectrum from the 2 hour static flow run shows that almost no diamond had been deposited onto the substrate. However, the broad graphite band at approximately 1499 cm<sup>-1</sup> shows much graphite has been deposited. Like the 2 hour flow run this was an unsuccessful growth run.

Overall the PDR method needs to be optimised to get some successful diamond growth. Using the conditions presented, diamond growth was highly unsuccessful.

## 9.2 Section B -OES

### 4 % Undoped Data Processing

This data was load level corrected, unlike the residually-doped data. Going through the spectra on the OES 'Waves' program, it was seen that the load level on the program was decreasing throughout the duration of the runs. One reason for this could be because graphitic residue was being deposited onto the window of the chamber, and as a result obstructing the OES lens. As the time increases during the run, deposition of graphite around the chamber would increase, this could explain the gradual decrease in the load level value. With this data having been load level corrected, as seen in **figure 27**, this provides a more precise representation of C<sub>2</sub> concentration during the run. The baseline for this data set was corrected relative to a peak at 519.4352 nm.

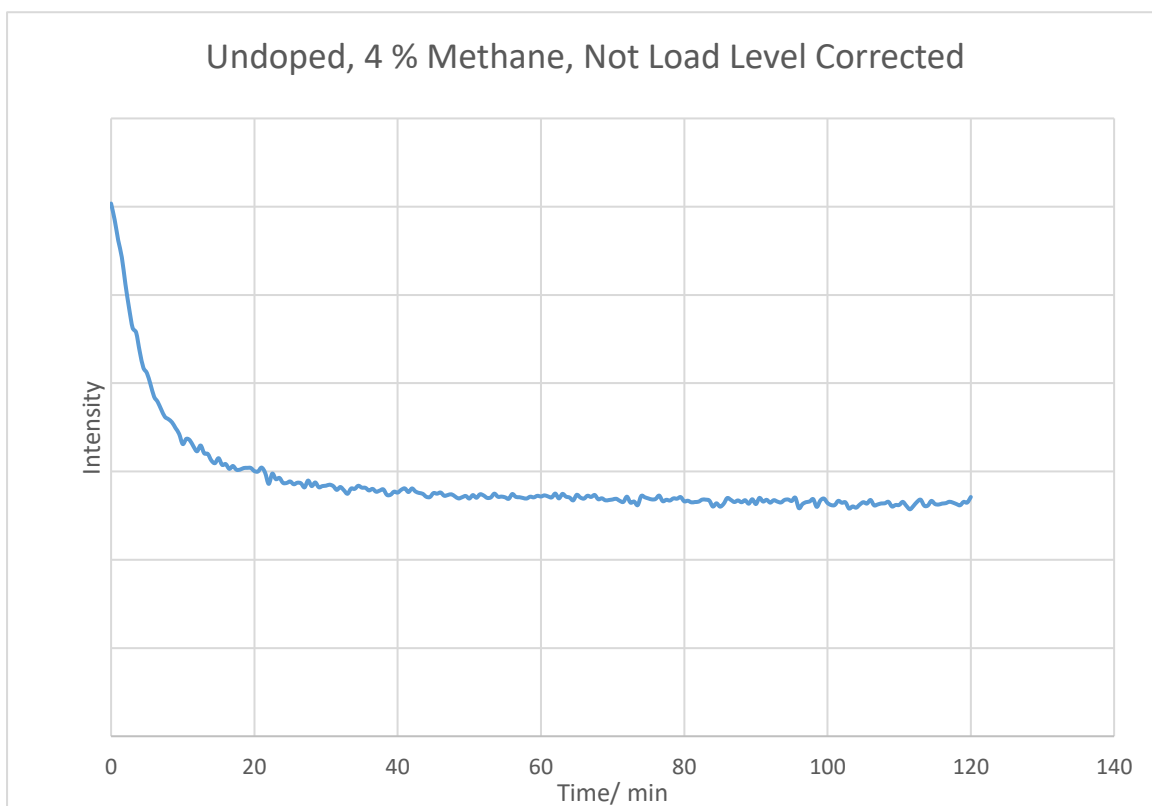


**Figure 37** OES result for the flow run in the undoped 4 % data set. This data having not been load level corrected.

**Figure 37** shows data from a flow run within this data set having been analysed using the exact same method as the residually-doped data sets. For a flow run, a constant C<sub>2</sub> intensity is expected to be seen as methane is being flown at a constant rate for the entirety of the run. The decrease shown in **figure 37** provided inconsistent results. Once this data had been load level corrected the C<sub>2</sub> peak was shown to be approximately constant, showing the necessity load level corrections in this data set.

## 6 % Undoped Data Processing

The undoped chamber was used with the OES lens directed through the top of the chamber onto the top of the plasma. However, when doing load level corrections, inconsistent results were outputted as shown. The load level corrected data for this set is shown in **figure 38**. The  $C_2$  intensity was shown not to decrease for approximately 12 minutes each time the precursor gases were added, which was unexpected. This is because as methane is deposited a gradual decrease would be observed. The reason for this inconsistency was that the methane peak had a higher intensity than the hydrogen Balmer- $\alpha$  peak. This was never the case for the previous data sets, even the 6 % residually-doped data set. This could be due to the OES lens looking at a different part of the plasma in this data set. The load level is set relative to the highest intensity peak within the spectrum.

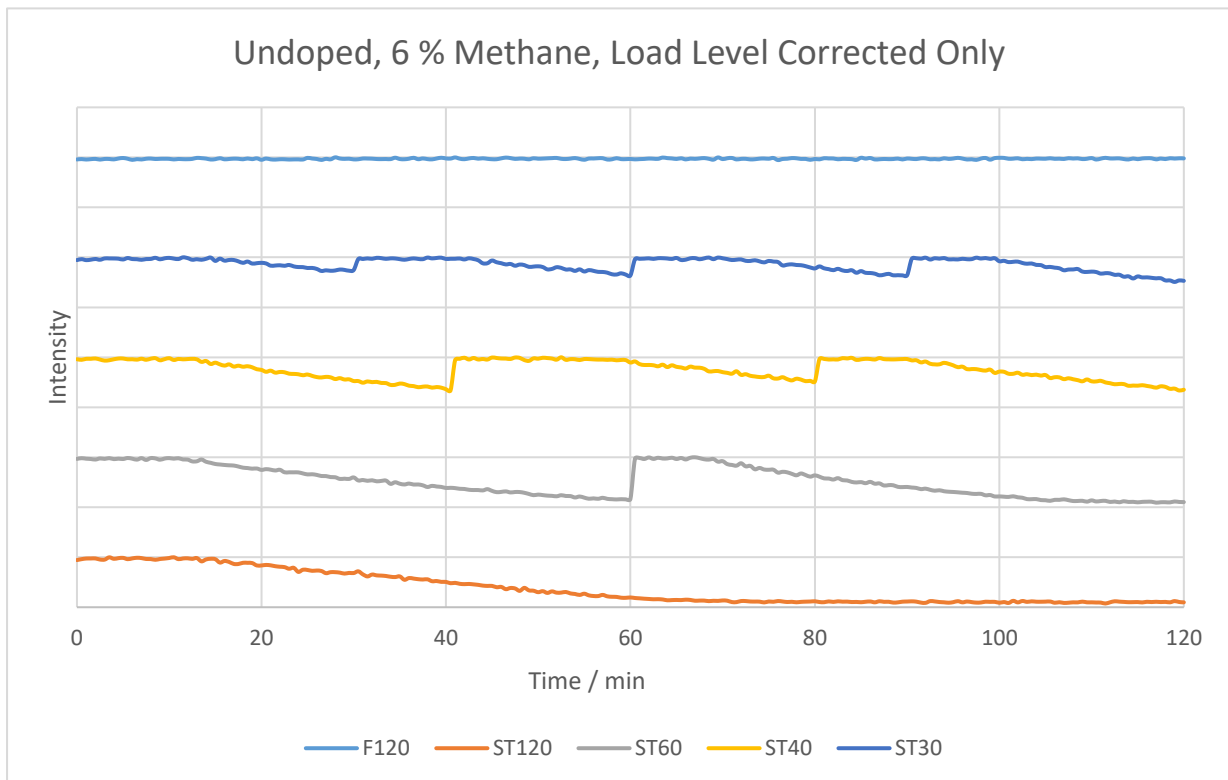


**Figure 38** OES results showing  $C_2$  concentration for the undoped 6 % data set.

The spectrometer can take 50,000 counts per wavelength per scan. The load level is the fraction of the number of counts for the highest intensity peak divided by the maximum number of counts. The intensity value of the  $C_2$  peak for each of the previous sets divided the number of counts taken by the detector for that wavelength by the load level. In this data, set the load level was set using the  $C_2$  as this was the highest intensity peak whenever the precursor gases were cycled in. Hence as the load level is relative to the highest intensity peak, the intensity value given by the spectrum will show a consistent level of  $C_2$  concentration. This is summarised in **equation 1** which shows how the  $C_2$  intensity value is calculated, if  $C_2$  is the highest intensity peak.

$$\frac{C_2}{(C_2/Max)} = C_2 \text{ intensity value}$$

Max = total number counts  
spectrometer can take

$C_2$  = number of  $C_2$  counts

**Equation 1** The load level calculation if  $C_2$  was the highest intensity peak.

This is until enough carbon is deposited that the intensity of the peak falls below the hydrogen Balmer- $\alpha$  peak. From this point the load level will begin taking values relative the hydrogen Balmer- $\alpha$  peak. To fix this problem, each run within this data set was corrected relative to the hydrogen- $\alpha$  peak.

### 9.3 Raman Analysis Data and Spectra

Table 11 showing all the Raman data for the runs conducted. In the 6 % residually-doped the corner value of ST30 was taken as there was uneven deposition. ST40 was omitted as the value wasn't fitted properly.

4% res					
<u>4 % Residually D</u>		<u>Centre</u>	<u>Width</u>	<u>Height</u>	<u>%Gaussian</u>
<b>F120</b>	<b>Diamond</b>	1330.64	10.9753	252132	52.06
	<b>Graphite</b>	1528.45	206.055	34641.2	100
<b>ST120</b>	<b>Diamond</b>	1330.96	9.65639	72025.6	42.1475
	<b>Graphite</b>	1469.75	355.677	27527.4	49.3493
<b>ST60</b>	<b>Diamond</b>	1331.32	9.27384	165965	15.8721
	<b>Graphite</b>	1499.93	205.714	96.3824	96.3824
<b>ST40</b>	<b>Diamond</b>	1330.78	9.11783	171149	39.9276
	<b>Graphite</b>	1500.29	261.786	17891.5	100
<b>ST30</b>	<b>Diamond</b>	1331.19	9.81159	152763	57.0043
	<b>Graphite</b>	1502.64	139.338	36673.6	29.1951
<b>Average</b>			9.76699		

6% res					
		<u>Centre</u>	<u>Width</u>	<u>Height</u>	<u>%Gaussian</u>
<b>F120</b>	<b>Diamond</b>	1331.39	11.6896	17773.9	50.9945
	<b>Graphite</b>	1556.22	253.709	579.65	50.6521
<b>ST120</b>	<b>Diamond</b>	1330.9	9.05079	108246	25.6914
	<b>Graphite</b>	1488.88	308.272	24966.5	100
<b>ST60</b>	<b>Diamond</b>	1332.12	9.38957	184521	62.9233
	<b>Graphite</b>	1555.39	191.331	35344.2	49.7665
<b>ST40</b>	<b>Diamond</b>	1341.69	152.277	10210.5	46.808
	<b>Graphite</b>	1523.79	151.606	12120.3	52.6358
<b>ST30</b>	<b>Diamond</b>	1334.33	124.847	100964	100
	<b>Graphite</b>	1517.84	167.255	127665	100
<b>ST30 Corner</b>	<b>Diamond</b>	1331.2	11.0775	12146.6	
	<b>Graphite</b>	1404.2	2.37972	2081.11	
<b>Average</b>			10.30187		

4% undoped					
		<u>Centre</u>	<u>Width</u>	<u>Height</u>	<u>%Gaussian</u>
<b>F120</b>	<b>Diamond</b>	1331.12	9.71776	144745	11.5291
	<b>Graphite</b>	1535.66	265.851	23537.4	93.2716
<b>ST120</b>	<b>Diamond</b>	1330.94	10.1481	149349	100
	<b>Graphite</b>	1528.12	271.43	10786.2	50
<b>ST60</b>	<b>Diamond</b>	1331.47	9.29656	189360	74.2435
	<b>Graphite</b>	1521.16	140.015	28232.9	7.93637
<b>ST40</b>	<b>Diamond</b>	1331.51	9.56975	186029	100
	<b>Graphite</b>	1517.58	149.197	19795.7	48.5472
<b>ST30</b>	<b>Diamond</b>	1331.19	9.78413	151658	64.9455
	<b>Graphite</b>	1504.37	132.116	35099.2	29.6135
<b>Average</b>			9.70326		

6% Undoped					
		<u>Centre</u>	<u>Width</u>	<u>Height</u>	<u>%Gaussian</u>
<b>F120</b>	<b>Diamond</b>	1331.46	8.10771	287035	60.7031
	<b>Graphite</b>	1540.16	1552.052	32281.2	100
<b>ST120</b>	<b>Diamond</b>	1331.62	10.5024	135562	48.4749
	<b>Graphite</b>	1539.75	118.496	20687.6	48.7365
<b>ST60</b>	<b>Diamond</b>	1331.29	8.21294	18741.9	53.4455
	<b>Graphite</b>	1497.04	117.186	8346.02	21.722
<b>ST40</b>	<b>Diamond</b>	1331.01	11.2918	186277	62.6392
	<b>Graphite</b>	1398.76	170.433	53214.3	96.7984
<b>ST30</b>	<b>Diamond</b>	1330.87	8.42755	282477	44.1786
	<b>Graphite</b>	1468.34	170.381	29760.1	20.2828
<b>Average</b>			9.30848		

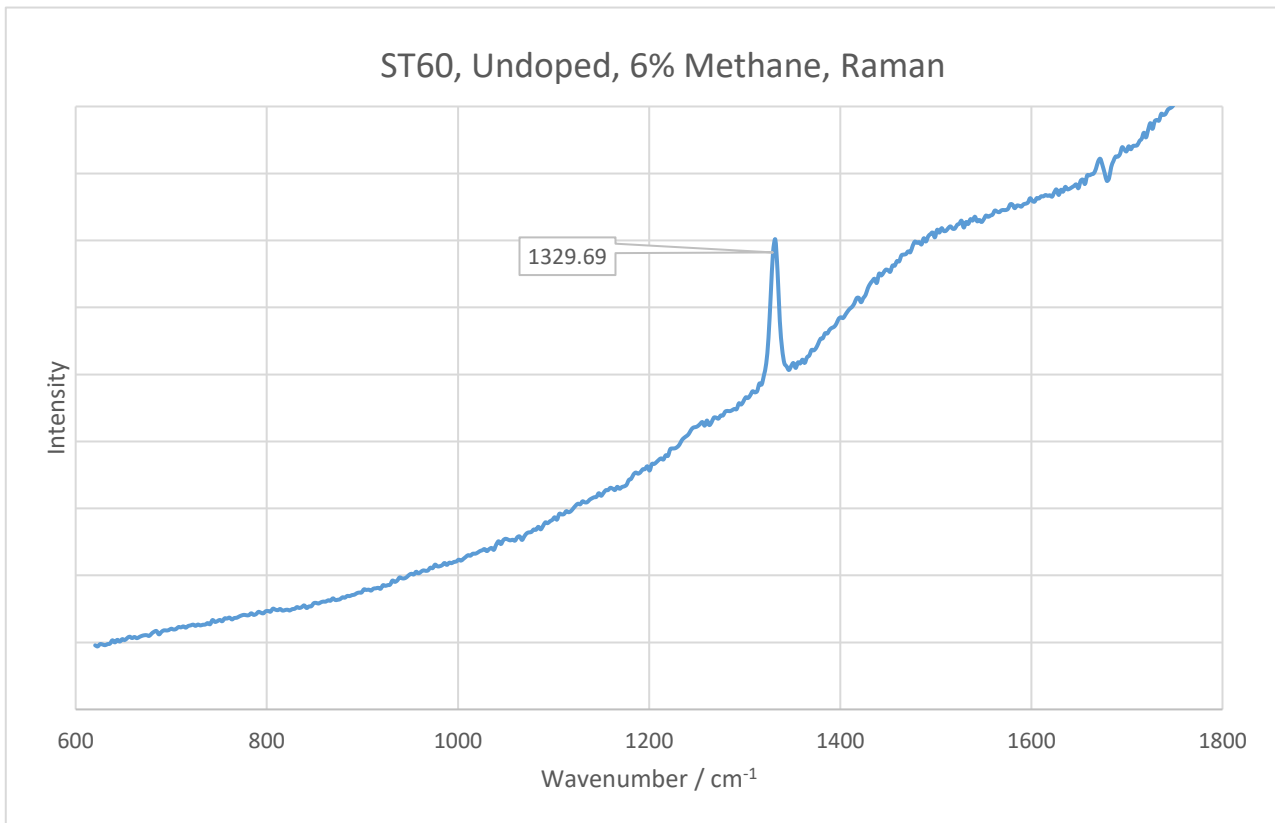


**Figure 39** Raman spectrum from the 6 % undoped ST60 run. This provided the most crystalline diamond out of the static runs. The diamond peak highlighted at 1329.69 cm<sup>-1</sup>.

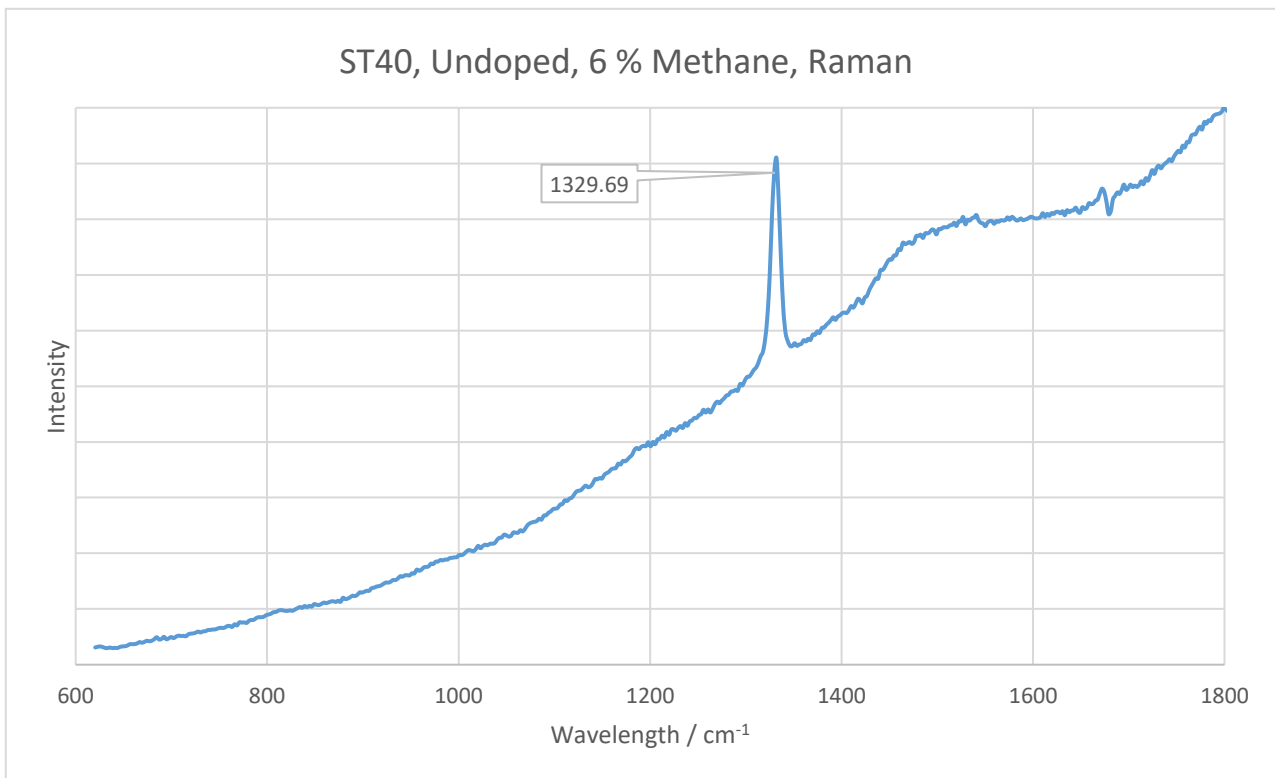


**Figure 40** Raman spectrum from the 6 % undoped ST40 run. This provided the least crystalline diamond out of the static runs. The diamond peak highlighted at 1329.69 cm<sup>-1</sup>.

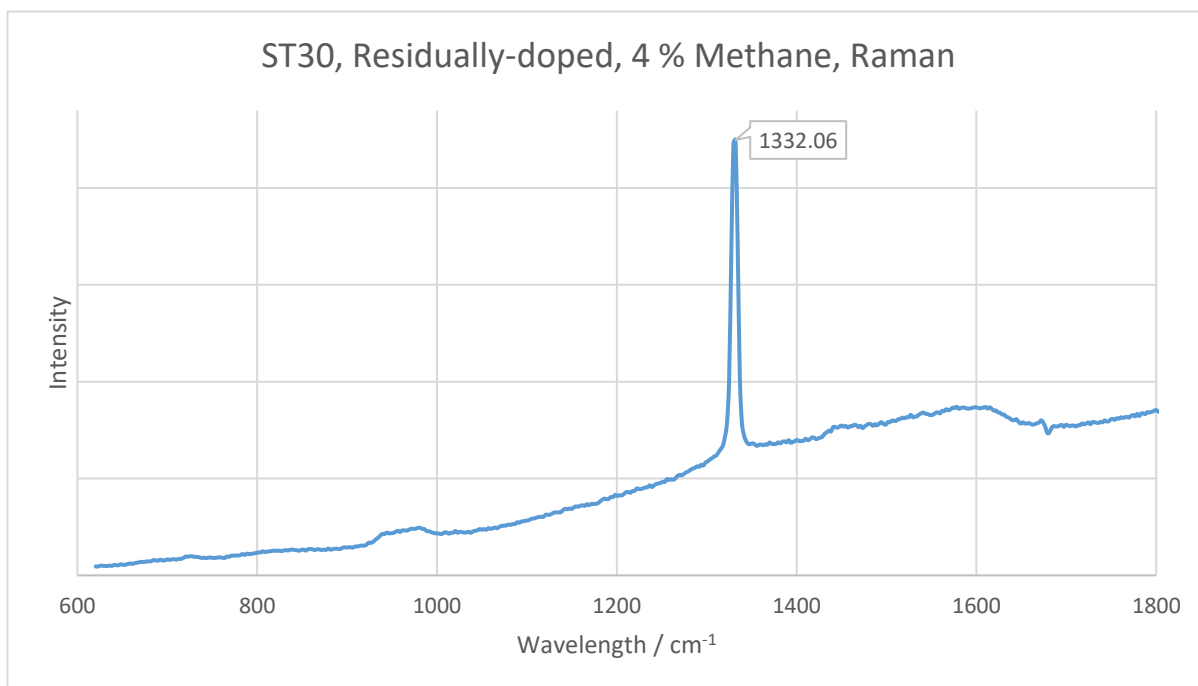


**Figure 41** Raman spectrum from the 4 % residually-doped ST30 run. This provided the least graphitic diamond growth out of the static runs. The diamond peak highlighted at 1332.06 cm<sup>-1</sup>.

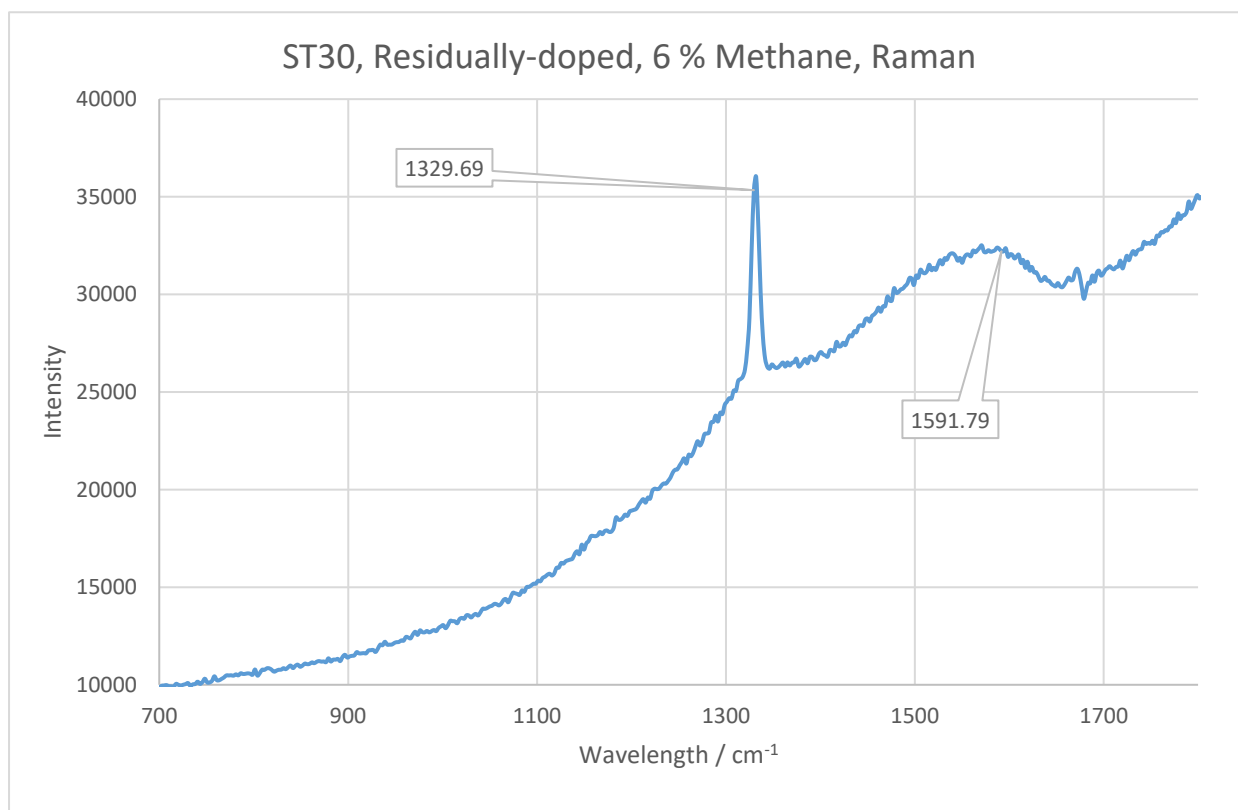


**Figure 42** Raman spectrum from the 6 % residually-doped ST30 run. This provided the most graphitic diamond growth out of the static runs. The diamond peak highlighted at 1329.69 cm<sup>-1</sup> and graphite band highlighted at approximately 1500 - 1700 cm<sup>-1</sup>.

## 9.4 Section D- SEM Images

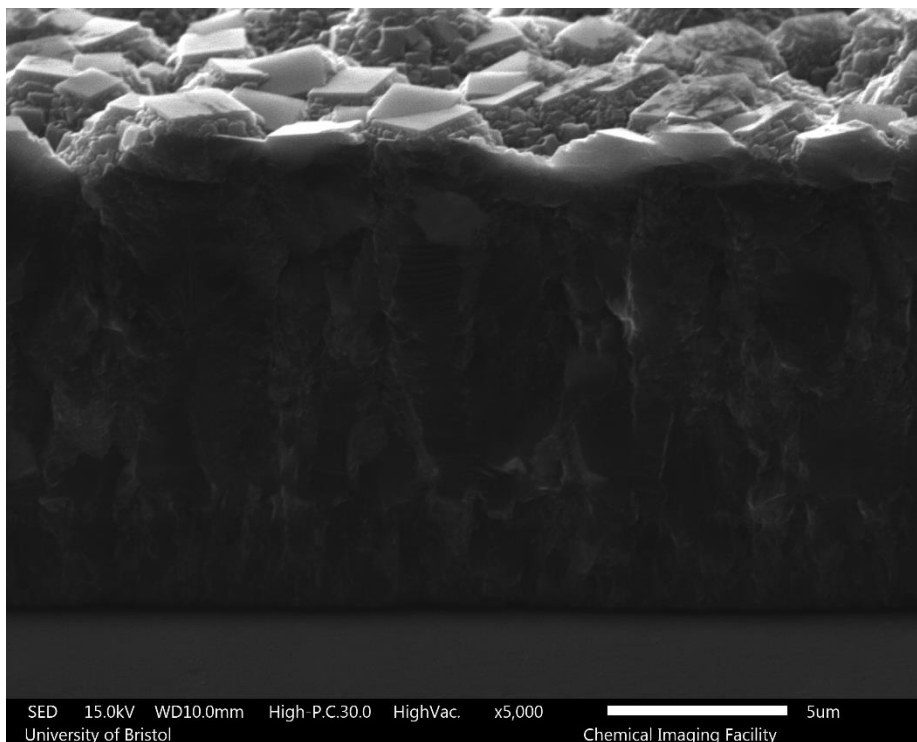


**Figure 43** Cross sectional SEM image taken from residually-doped, 6 % methane, ST40. This was taken from the middle of the sample and provided the highest growth rate out of the static cycles.

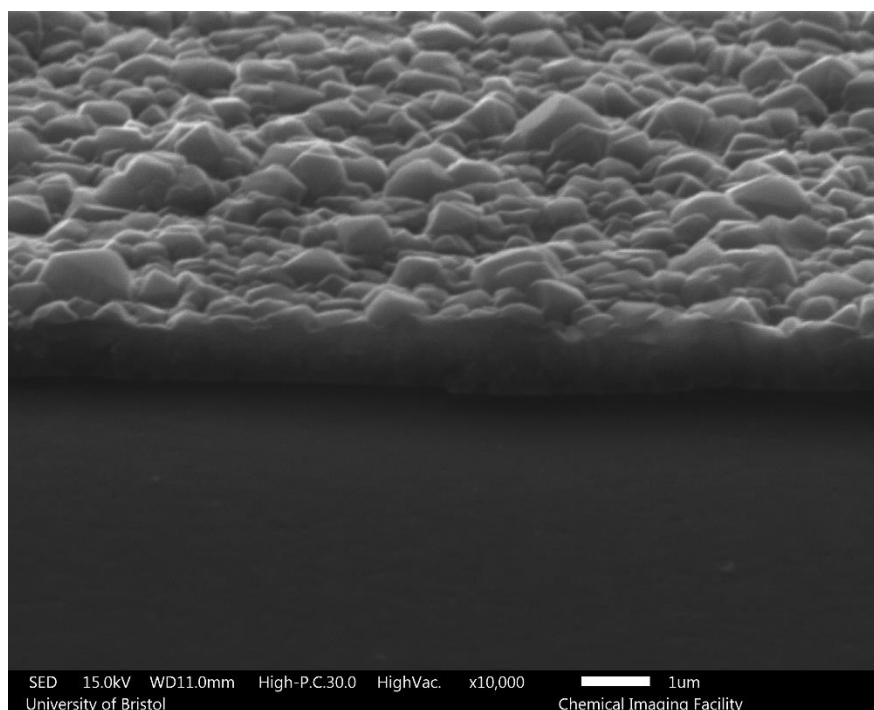


**Figure 44** Cross sectional SEM image taken from residually-doped, 4 % methane, ST120. This was taken from the middle of the sample and provided the lowest growth rate out of the static cycles.

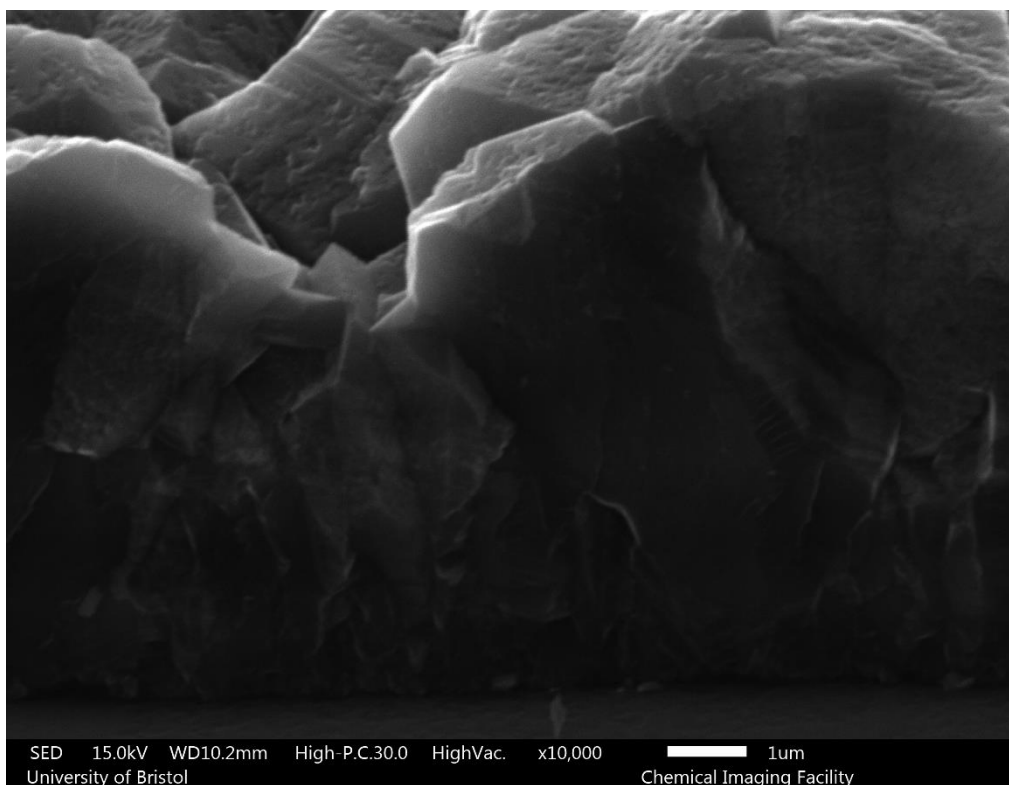


**Figure 45** Cross sectional SEM image taken from undoped, 4 % methane, ST120. This was taken from the edge of the sample. This sample provided one of the most uniform diamond films.

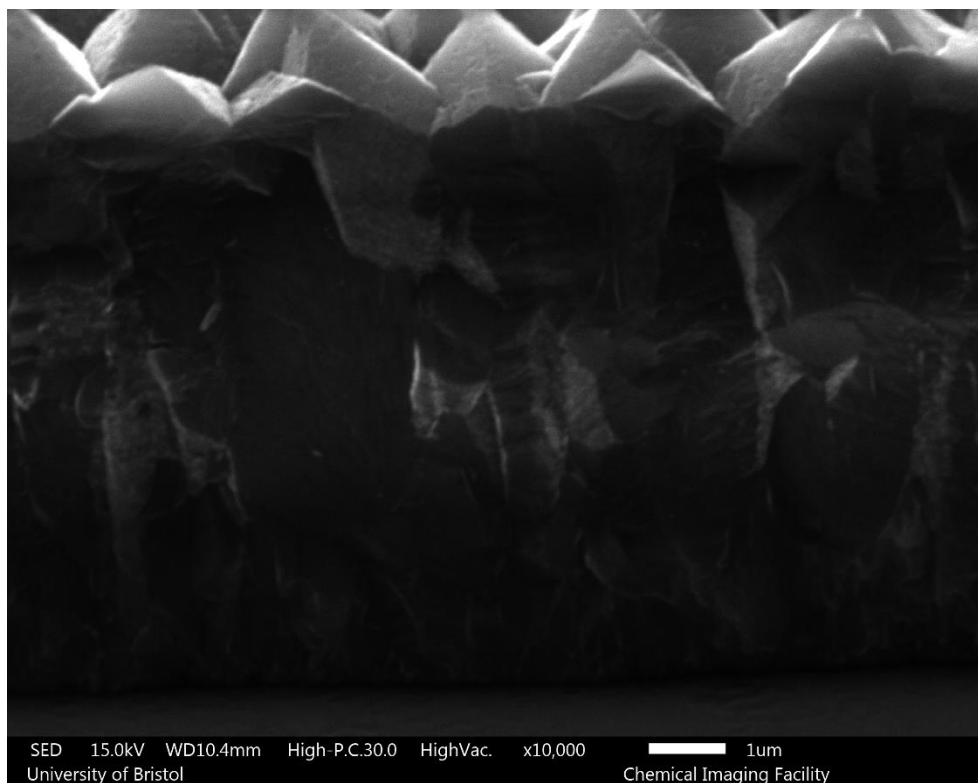


**Figure 46** Cross sectional SEM image taken from undoped, 4 % methane, ST120. This was taken from the middle of the sample. This sample provided one of the most uniform diamond films.

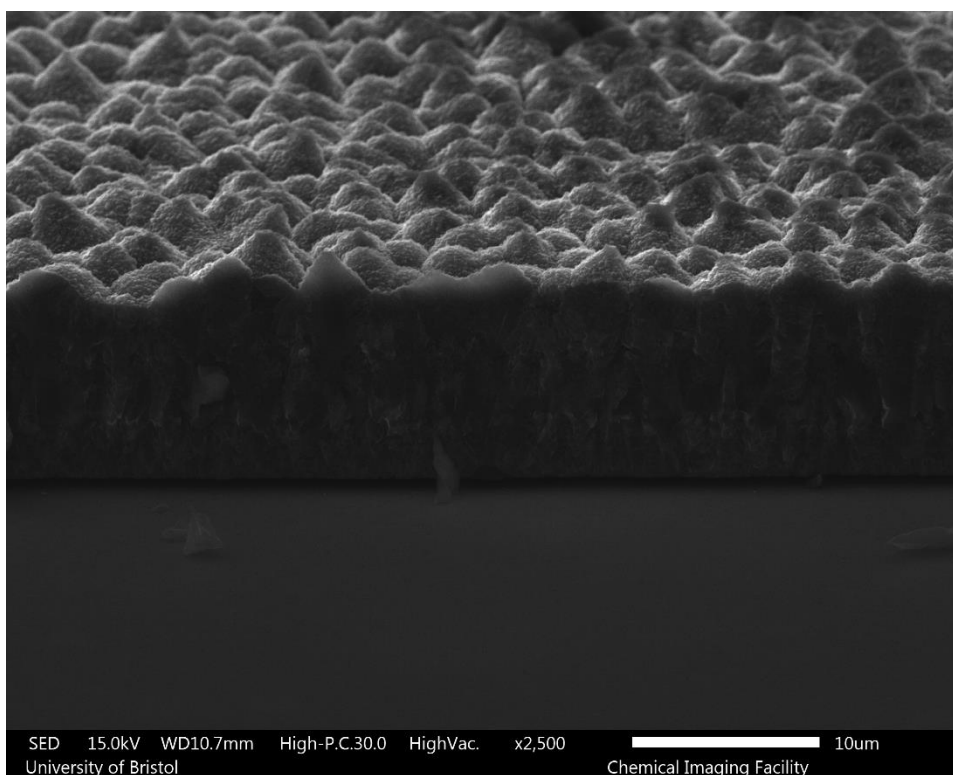


**Figure 47** Cross sectional SEM image taken from residually-doped, 6 % methane, ST40. This was taken from the edge of the sample. This sample provided one of the least diamond films.

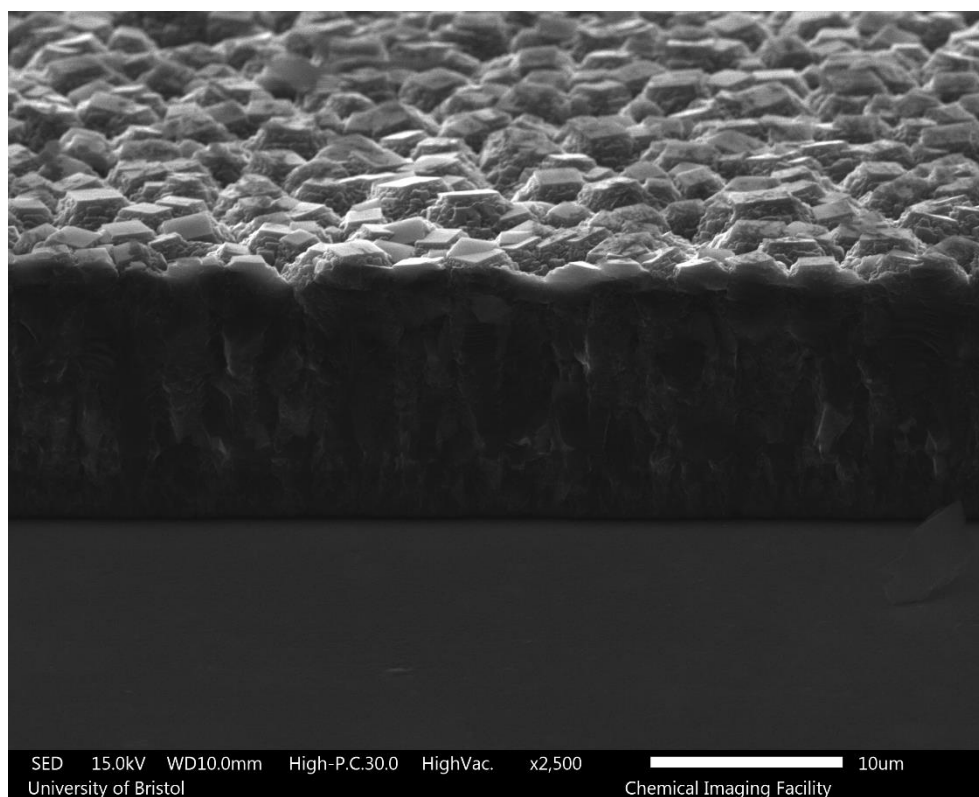


**Figure 48** Cross sectional SEM image taken from residually-doped, 6 % methane, ST40. This was taken from the middle of the sample. This sample provided one of the least diamond films.